root ganglia in mice, and mutation of human *PHF8* causes inherited X-linked mental retardation (Hasenpusch-Theil et al. 1999; Laumonnier et al. 2005; Abidi et al. 2007; Koivisto et al. 2007). Our results showed that KDM7 is expressed predominantly in the brain of fish and mice as well as in mammalian neuronal cells and is essential for development of the fish brain, suggesting that transcriptional regulation of the follistatin gene by KDM7 may be evolutionarily conserved. Functions in neuronal development based on their demethylase activity may thus be common to this class of JmjC domain-containing proteins.

Materials and methods

In vitro histone demethylase assays

We performed in vitro demethylation assays with the use of purified recombinant proteins and various forms of histone substrates. Demethylase activity was detected by measurement of formaldehyde release, immunoblot analysis with a series of methylation-specific antibodies (Supplemental Table S1), or matrix-assisted laser desorption ionization (MALDI)–time-of-flight (TOF) mass spectrometry, as detailed in the Supplemental Material.

In situ hybridization

Whole-mount zebrafish embryos were subjected to in situ hybridization under standard conditions with digoxigenin-labeled antisense RNA probes prepared from zebrafish *kdm7a* (XM_687822), *kdm7b* (XM_681621), or follistatin 1 (DQ317968) genes.

Other methods

Details of other procedures are provided in the Supplemental Material.

Acknowledgments

We thank B.D. Strahl for providing pCAL-SpSet2, National BioResource Project ZEBRAFISH for providing *HuC:Kaede* transgenic fish, and members of our laboratories for discussion. This work was supported in part by a grant from the Ministry of Education, Culture, Sports, Science, and Technology of Japan.

References

Abidi FE, Miano MG, Murray JC, Schwartz CE. 2007. A novel mutation in the PHF8 gene is associated with X-linked mental retardation with cleft lip/cleft palate. *Clin Genet* **72:** 19–22.

Allis CD, Berger SL, Cote J, Dent S, Jenuwien T, Kouzarides T, Pillus L, Reinberg D, Shi Y, Shiekhattar R, et al. 2007. New nomenclature for chromatin-modifying enzymes. *Cell* **131:** 633–636.

Bannister AJ, Schneider R, Kouzarides T. 2002. Histone methylation: Dynamic or static? *Cell* **109:** 801–806.

Cloos PA, Christensen J, Agger K, Helin K. 2008. Erasing the methyl mark: Histone demethylases at the center of cellular differentiation and disease. *Genes & Dev* **22:** 1115–1140.

Hasenpusch-Theil K, Chadwick BP, Theil T, Heath SK, Wilkinson DG, Frischauf AM. 1999. PHF2, a novel PHD finger gene located on human chromosome 9q22. *Mamm Genome* **10:** 294–298.

Hemmati-Brivanlou A, Kelly OG, Melton DA. 1994. Follistatin, an antagonist of activin, is expressed in the Spemann organizer and displays direct neuralizing activity. *Cell* **77:** 283–295.

Iwase S, Lan F, Bayliss P, de la Torre-Ubieta L, Huarte M, Qi HH, Whetstine JR, Bonni A, Roberts TM, Shi Y. 2007. The X-linked mental retardation gene SMCX/JARID1C defines a family of histone H3 lysine 4 demethylases. *Cell* **128:** 1077–1088.

Klose RJ, Kallin EM, Zhang Y. 2006a. JmjC-domain-containing proteins and histone demethylation. *Nat Rev Genet* **7:** 715–727.

Klose RJ, Yamane K, Bae Y, Zhang D, Erdjument-Bromage H, Tempst P, Wong J, Zhang Y. 2006b. The transcriptional repressor JHDM3A demethylates trimethyl histone H3 lysine 9 and lysine 36. *Nature* **442:** 312–316.

Koivisto AM, Ala-Mello S, Lemmela S, Komu HA, Rautio J, Jarvela I. 2007. Screening of mutations in the PHF8 gene and identification of a novel mutation in a Finnish family with XLMR and cleft lip/cleft palate. *Clin Genet* **72:** 145–149.

Lachner M, O'Sullivan RJ, Jenuwein T. 2003. An epigenetic road map for histone lysine methylation. *J Cell Sci* **116:** 2117–2124.

Lan F, Nottke AC, Shi Y. 2008. Mechanisms involved in the regulation of histone lysine demethylases. *Curr Opin Cell Biol* **20:** 316–325.

Laumonnier F, Holbert S, Ronce N, Faravelli F, Lenzner S, Schwartz CE, Lespinasse J, Van Esch H, Lacombe D, Goizet C, et al. 2005. Mutations in PHF8 are associated with X linked mental retardation and cleft lip/cleft palate. *J Med Genet* **42:** 780–786.

Lin SY, Morrison JR, Phillips DJ, de Kretser DM. 2003. Regulation of ovarian function by the TGF-β superfamily and follistatin. *Reproduction* **126:** 133–148.

Margueron R, Trojer P, Reinberg D. 2005. The key to development: Interpreting the histone code? *Curr Opin Genet Dev* **15:** 163–176.

Martin C, Zhang Y. 2005. The diverse functions of histone lysine methylation. *Nat Rev Mol Cell Biol* **6:** 838–849.

Robu ME, Larson JD, Nasevicius A, Beiraghi S, Brenner C, Farber SA, Ekker SC. 2007. p53 activation by knockdown technologies. *PLoS Genet* **3:** e78. doi: 10.1371/journal.pgen.0030078.

Sato T, Takahoko M, Okamoto H. 2006. HuC:Kaede, a useful tool to label neural morphologies in networks in vivo. *Genesis* **44:** 136–142.

Shi Y, Whetstine JR. 2007. Dynamic regulation of histone lysine methylation by demethylases. *Mol Cell* **25:** 1–14.

Shi Y, Lan F, Matson C, Mulligan P, Whetstine JR, Cole PA, Casero RA, Shi Y. 2004. Histone demethylation mediated by the nuclear amine oxidase homolog LSD1. *Cell* **119:** 941–953.

Strahl BD, Allis CD. 2000. The language of covalent histone modifications. *Nature* **403:** 41–45.

Tsukada Y, Fang J, Erdjument-Bromage H, Warren ME, Borchers CH, Tempst P, Zhang Y. 2006. Histone demethylation by a family of JmjC domain-containing proteins. *Nature* **439:** 811–816.

Whetstine JR, Nottke A, Lan F, Huarte M, Smolikov S, Chen Z, Spooner E, Li E, Zhang G, Colaiacovo M, et al. 2006. Reversal of histone lysine trimethylation by the JMJD2 family of histone demethylases. *Cell* **125:** 467–481.

Zhu CC, Boone JQ, Jensen PA, Hanna S, Podemski L, Locke J, Doe CQ, O'Connor MB. 2008. *Drosophila* Activin- and the Activin-like product Dawdle function redundantly to regulate proliferation in the larval brain. *Development* **135:** 513–521.

ARTICLES

Skp2 targeting suppresses tumorigenesis by *Arf-p53*-independent cellular senescence

Hui-Kuan Lin[1,2,3], Zhenbang Chen[1,2,4]†, Guocan Wang[1,2,4]*, Caterina Nardella[1,2,4]*, Szu-Wei Lee[3]*, Chan-Hsin Chan[3], Wei-Lei Yang[3], Jing Wang[3], Ainara Egia[4], Keiichi I. Nakayama[5], Carlos Cordon-Cardo[2]†, Julie Teruya-Feldstein[2] & Pier Paolo Pandolfi[1,2,4]

Cellular senescence has been recently shown to have an important role in opposing tumour initiation and promotion. Senescence induced by oncogenes or by loss of tumour suppressor genes is thought to critically depend on induction of the $p19^{Arf}$–p53 pathway. The Skp2 E3-ubiquitin ligase can act as a proto-oncogene and its aberrant overexpression is frequently observed in human cancers. Here we show that although *Skp2* inactivation on its own does not induce cellular senescence, aberrant proto-oncogenic signals as well as inactivation of tumour suppressor genes do trigger a potent, tumour-suppressive senescence response in mice and cells devoid of *Skp2*. Notably, *Skp2* inactivation and oncogenic-stress-driven senescence neither elicit activation of the $p19^{Arf}$–p53 pathway nor DNA damage, but instead depend on Atf4, p27 and p21. We further demonstrate that genetic *Skp2* inactivation evokes cellular senescence even in oncogenic conditions in which the $p19^{Arf}$–p53 response is impaired, whereas a Skp2–SCF complex inhibitor can trigger cellular senescence in p53/Pten-deficient cells and tumour regression in preclinical studies. Our findings therefore provide proof-of-principle evidence that pharmacological inhibition of Skp2 may represent a general approach for cancer prevention and therapy.

Cellular senescence represents an irreversible form of cell-cycle arrest that can be triggered by a variety of insults. Induction of cellular senescence (for example, by oncogenic Ras) results in $p19^{Arf}$ (encoded by the *Ink4a/Arf* locus, also known as *Cdkn2a* locus) and p53 accumulation, which is critical for this senescence response. Recent studies suggest that cellular senescence can act as an important tumour-suppressive mechanism to restrict tumour development *in vivo*[1–7].

Inactivation of Pten functions is frequently observed in human cancers[8–10]. Although Pten negatively regulates cell proliferation and survival, we surprisingly discovered that acute *Pten* inactivation triggers the accumulation of $p19^{Arf}$–p53 and cellular senescence[2]. Concomitant inactivation of *p53* (also known as *Trp53* in mice, and *TP53* in humans) and *Pten* abrogates this senescence response, in turn promoting invasive and lethal prostate cancer[2]. Although these findings further underscore the critical importance of the cellular senescence *Arf-p53* failsafe pathway, the frequent loss or mutation of *ARF* or *P53* in human cancers would compromise the tumour-suppressive efficacy of this response, thereby limiting therapeutic potential.

Skp2 is a critical component of the Skp2–SCF complex, which acts as an E3 ligase to target p27 and other substrates for ubiquitylation and degradation[11,12]. Recent studies suggest that Skp2 may have oncogenic activity[13–16]. Notably, SKP2 overexpression is frequently observed in human cancer[11,12,17], strongly suggesting that SKP2 overexpression may contribute to tumorigenesis. *Skp2*-knockout mice are viable and fertile[18]. Hence, specific inactivation of *Skp2* may represent an appealing therapeutic modality. Here we show that *Skp2* inactivation profoundly restricts tumorigenesis by eliciting cellular senescence only in oncogenic conditions. Remarkably, this senescence response is triggered in a $p19^{Arf}$–p53-independent manner. Skp2 pharmacological inactivation may therefore represent a general approach towards a 'pro-senescence' therapy for cancer prevention and treatment.

Skp2 loss restores cellular senescence by Ras and E1A

Skp2 deficiency delays cell cycle progression[11,12]. We therefore asked whether *Skp2* deficiency would trigger cellular senescence. We isolated mouse embryonic fibroblasts (MEFs) from wild-type and $Skp2^{-/-}$ mice and determined cellular senescence in these cells by senescence-associated β-galactosidase (SA-β-gal) staining. Although $Skp2^{-/-}$ MEFs proliferated less than wild-type MEFs (Supplementary Fig. 1e)[11,12], cellular senescence in $Skp2^{-/-}$ MEFs was comparable to that in the wild-type MEFs (Supplementary Fig. 1a). In contrast, acute inactivation of *Pten* in MEFs markedly increased cellular senescence as previously reported (Supplementary Fig. 1a)[2]. Thus, *Skp2* deficiency by itself does not elicit cellular senescence.

Ectopic overexpression of proto-oncogenic Ras (Ras(G12V)) in MEFs elicits cellular senescence through the $p19^{Arf}$–p53 pathway[19,20]. Simultaneous co-expression of E1A and Ras in MEFs overcomes Ras-induced senescence by preventing activation of the $p19^{Arf}$–p53 pathway and resulting in oncogenic transformation[20]. Thus, E1A enables Ras to overcome the cellular senescence response. As Skp2 also cooperates with oncogenic Ras to induce cell transformation[13], it is conceivable that Skp2 might also display its oncogenic activity by antagonizing Ras-induced cellular senescence. On this basis, we tested whether endogenous Skp2 activity is required for cellular transformation induced by Ras and E1A. Although cellular senescence was not

[1]Cancer Biology and Genetics Program, [2]Department of Pathology, Sloan-Kettering Institute, Memorial Sloan-Kettering Cancer Center, 1275 York Avenue, New York, New York 10021, USA. [3]Department of Molecular and Cellular Oncology, The University of Texas M.D. Anderson Cancer Center, Houston, Texas 77030, USA. [4]Cancer Genetics Program, Beth Israel Deaconess Cancer Center and Department of Medicine, Beth Israel Deaconess Medical Center, Harvard Medical School, 330 Brookline Avenue, Boston, Massachusetts 02215, USA. [5]Department of Molecular and Cellular Biology, Medical Institute of Bioregulation, Kyushu University, Fukuoka, Fukuoka 812-8582, Japan. †Present addresses: Department of Biochemistry and Cancer Biology, Meharry Medical College, 1005 Dr D. B. Todd Jr Boulevard, Nashville, Tennessee 37208-3599, USA (Z.C.); Irving Cancer Research Center, Room 309, 1130 St. Nicholas Avenue, New York, New York 10032, USA (C.C.-C.).
*These authors contribute equally to this work.

observed in wild-type MEFs after Ras and E1A overexpression, *Skp2* deficiency triggered cellular senescence (Supplementary Fig. 1b, c). We also found that the ability of Ras to induce cellular senescence was far greater in $Skp2^{-/-}$ MEFs than in wild-type MEFs (Supplementary Fig. 1b, c). It should be noted that the induction of $p19^{Arf}$ and p53 protein levels in $Skp2^{-/-}$ MEFs by Ras was comparable if not lower than that of wild-type MEFs (Supplementary Fig. 1d). Moreover, *Skp2* inactivation profoundly restricted cell proliferation and transformation after Ras and E1A overexpression (Supplementary Fig. 1e, f). Thus, *Skp2* inactivation triggers cellular senescence in the presence of powerful oncogenic signals, even when the $p19^{Arf}$–p53 response is evaded.

Skp2 loss causes senescence in $Pten^{+/-}$ and $Arf^{-/-}$ mutants

We assessed whether *Skp2* inactivation would trigger cellular senescence even when cells experience loss of major tumour-suppressive networks such as those controlled by Pten and $p19^{Arf}$–p53. To this end, we crossed $Skp2^{-/-}$ mutants with $Pten^{+/-}$ and $Arf^{-/-}$ mutants. The resulting compound mice were further intercrossed to generate MEFs of different genotypes for cell proliferation and senescence assays. As aforementioned, $Skp2^{-/-}$ MEFs grew much slower than wild-type MEFs, whereas wild-type and $Pten^{+/-}$ MEFs grew comparably (Supplementary Fig. 2a). No obvious cellular senescence was observed in wild-type, $Pten^{+/-}$ and $Skp2^{-/-}$ MEFs (Fig. 1a). Surprisingly, $Pten^{+/-}$ $Skp2^{-/-}$ MEFs had a slower growth rate than $Skp2^{-/-}$ MEFs and exhibited full-blown characteristics of cellular senescence such as flattened large cells and positive SA-β-gal staining (Fig. 1a and Supplementary Fig. 2a). We also detected cellular senescence in $Pten^{+/-}$ $Skp2^{-/-}$ MEFs under hypoxic conditions (Supplementary Fig. 2b). We did not see cooperation between *Pten* inactivation and *Skp2* deficiency in triggering apoptosis, although $Skp2^{-/-}$ MEFs had a higher rate of apoptosis than wild-type MEFs (Supplementary Fig. 3a)[18]. However, the apoptosis rate in the prostate of $Pten^{+/-}$ $Skp2^{-/-}$ mice was higher than in wild-type, $Pten^{+/-}$ and $Skp2^{-/-}$ mice (see later and Supplementary Fig. 3b).

As cellular senescence is largely dependent on activation of the $p19^{Arf}$–p53 pathway in MEFs[2,21,22], we determined whether this pathway is activated in $Pten^{+/-}$ $Skp2^{-/-}$ MEFs. Notably, we found that $p19^{Arf}$ and p53 protein levels in $Pten^{+/-}$ $Skp2^{-/-}$ MEFs were comparable to levels in wild-type MEFs (Fig. 1b and Supplementary Fig. 4), suggesting that the $p19^{Arf}$–p53 pathway may not be involved in the senescence response in $Pten^{+/-}$ $Skp2^{-/-}$ MEFs. To test this hypothesis further, we exposed MEFs of various genotypes to two well-established p53-inactivating tools: a short hairpin RNA (shRNA) against *p53* (ref. 23) or a dominant-negative p53 mutant (p53-DN)[24]. Notably, in both conditions cell growth was promoted in wild-type and $Pten^{-/-}$ MEFs (Supplementary Fig. 5a, b), but neither of them overcame the cellular senescence nor the growth arrest in $Pten^{+/-}$ $Skp2^{-/-}$ MEFs (Fig. 1c and Supplementary Fig. 5c), suggesting that *Skp2*-deficiency cooperates with *Pten* inactivation to trigger a new senescence response by a $p19^{Arf}$–p53-independent pathway.

$p19^{Arf}$ induction is required for cellular senescence in MEFs in the context of acute *Pten* inactivation[25], whereas loss of $p19^{Arf}$ leads to cell immortalization[2,21,22]. We investigated whether *Skp2* inactivation could elicit cellular senescence in an *Arf*-deficient genetic background. Notably, $Arf^{-/-}$ $Skp2^{-/-}$ MEFs showed massive cellular senescence similar to $Pten^{+/-}$ $Skp2^{-/-}$ MEFs (Fig. 1d). Moreover, p53 expression was not induced in $Arf^{-/-}$ $Skp2^{-/-}$ MEFs (Supplementary Fig. 6a). This cellular senescence profoundly suppressed the growth of $Arf^{-/-}$ MEFs (Supplementary Fig. 6b). *Skp2* deficiency also induced cellular senescence after p53 inactivation (Supplementary Fig. 6c, d).

DNA damage has been recently associated with cellular senescence[26–28]. However, we found no evidence of DNA-damage-response activation in $Pten^{+/-}$ $Skp2^{-/-}$ MEFs, as determined by the levels of phosphorylated-(S15)-p53 and -γ-H2ax (also known as γ-H2afx) (Supplementary Fig. 4). Collectively, these results support the notion that *Skp2* inactivation can trigger a new type of cellular senescence that does not involve DNA damage and can suppress transformation even when the $p19^{Arf}$–p53 response is impaired.

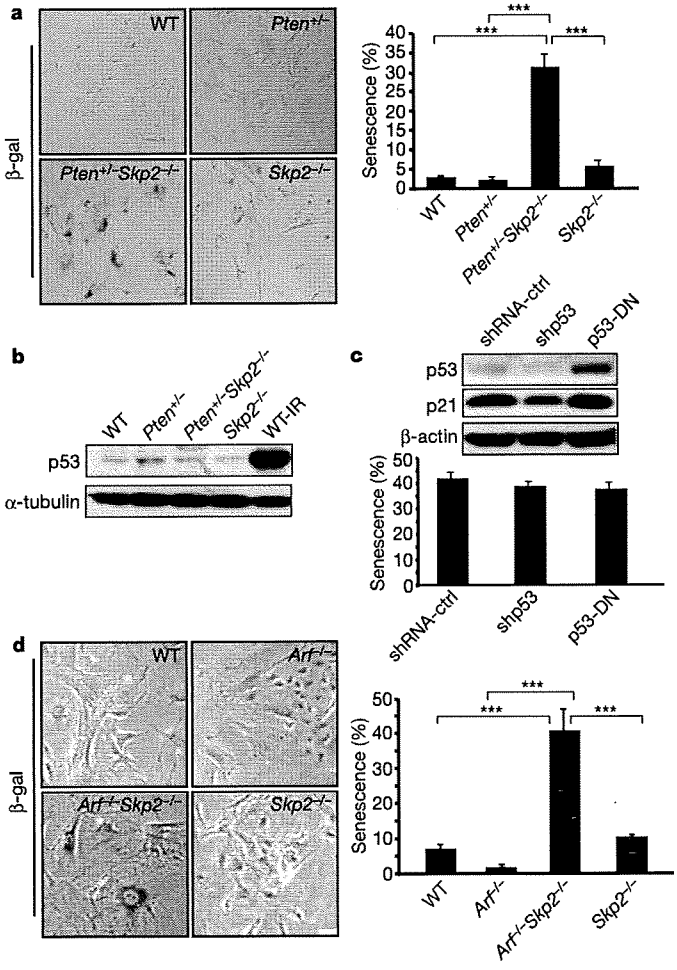

Figure 1 | *Skp2* loss triggers a new senescence response in MEFs in the context of *Pten* inactivation and *Arf* deficiency by a $p19^{Arf}$–p53-independent pathway. **a**, Primary MEFs at passage 5 from various mouse embryos were plated for senescence assay. WT, wild type. **b**, Cell lysates were collected from primary MEFs of various genotypes of mouse embryos for western blot analysis. The lysates from wild-type MEFs treated with γ-irradiation for 60 min served as a positive control for p53. **c**, Primary $Pten^{+/-}$ $Skp2^{-/-}$ MEFs infected with retroviruses expressing various control shRNA (shRNA-ctrl), *p53* shRNA (shp53), or dominant-negative p53 (p53-DN) were plated for senescence assay and western blot analysis. **d**, Primary MEFs at passage 5 from various genotypes of mouse embryos were plated for senescence assay. Results are presented as mean ± s.d. from a representative experiment performed in triplicate. $***P < 0.001$ using two-tailed Student's *t*-test, $n = 3$.

p27, p21 and Atf4 induction contribute to senescence

We next examined the molecular mechanism by which *Skp2* deficiency synergizes with oncogenic insults to trigger cellular senescence. Although p53 and $p19^{Arf}$ levels remained unchanged, we found that *Skp2* deficiency cooperated with *Pten* inactivation or *Arf* loss to induce p27 expression (Fig. 2a, b). p21 expression was also increased in $Pten^{+/-}$ $Skp2^{-/-}$ and $Arf^{-/-}$ $Skp2^{-/-}$ MEFs (Fig. 2a, b). E2F1, cyclin D1 and Cdt1, involved in cell cycle progression and DNA replication, are also targets for Skp2 (refs 12, 29). We found that cyclin D1, but not E2F1 and Cdt1, were induced in $Pten^{+/-}$ $Skp2^{-/-}$ MEFs (Supplementary Fig. 7a). Because cyclin D1 promotes cell cycle progression, its upregulation is unlikely to be involved in mediating senescence in $Pten^{+/-}$ $Skp2^{-/-}$ MEFs.

Endoplasmic reticulum (ER) stress proteins such as BiP (also known as Hspa5 or GRP78), phospho-Perk (p-Perk), and Atf4 are induced after oncogenic insults and have an important role in cellular

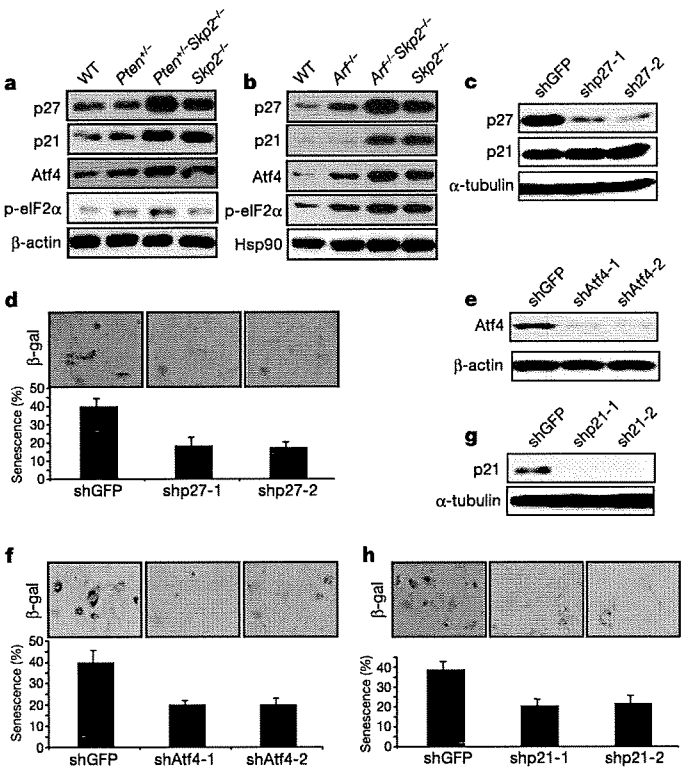

Figure 2 | Upregulation of p27, p21 and Atf4 drives cellular senescence in *Pten*$^{+/-}$ *Skp2*$^{-/-}$ and *Arf*$^{-/-}$ *Skp2*$^{-/-}$ MEFs. **a, b,** Cell lysates were collected from primary MEFs of various genotypes of mouse embryos for western blot analysis. **c, d,** *Pten*$^{+/-}$ *Skp2*$^{-/-}$ MEFs at passage 2 infected with lentiviruses expressing green fluorescent protein (GFP) shRNA (shGFP) or *p27* shRNA (shp27-1 and -2) were plated for western blot analysis (**c**) and senescence assay (**d**). Results are mean ± s.d. from a representative experiment performed in triplicate. **e, f,** *Pten*$^{+/-}$ *Skp2*$^{-/-}$ MEFs at passage 2 infected with lentiviruses expressing GFP shRNA or *Atf4* shRNA were plated for western blot analysis (**e**) and senescence assay (**f**). **g, h,** *Pten*$^{+/-}$ *Skp2*$^{-/-}$ MEFs at passage 2 infected with lentiviruses expressing GFP shRNA or *p21* shRNA were plated for western blot analysis (**g**) and senescence assay (**h**).

senescence[30]. We did not find a significant increase in BiP or p-Perk (Supplementary Fig. 7b and data not shown) in *Pten*$^{+/-}$ *Skp2*$^{-/-}$ MEFs. In contrast, Atf4 was markedly induced in *Pten*$^{+/-}$ *Skp2*$^{-/-}$ MEFs (Fig. 2a). Likewise, we also observed a marked increase in Atf4 protein levels, but not p-Perk, in *Arf*$^{-/-}$ *Skp2*$^{-/-}$ MEFs (Fig. 2b and Supplementary Fig. 7c). The induction of Atf4 protein levels in *Pten*$^{+/-}$ *Skp2*$^{-/-}$ MEFs was not accompanied by messenger RNA upregulation, nor by the enhanced Atf4 protein stability (Supplementary Fig. 8 and data not shown). Instead, we observed an increase in phosphorylated eIF2α (p-eIF2α; also known as p-Eif2s1) in *Pten*$^{+/-}$ *Skp2*$^{-/-}$ and *Arf*$^{-/-}$ *Skp2*$^{-/-}$ MEFs compared to wild-type cells (Fig. 2a, b). Because p-eIF2α positively regulates Atf4 translation[31], our results indicate that Atf4 upregulation is probably triggered by the enhancement of p-eIF2α levels.

As p27, p21 and Atf4 were induced in both *Pten*$^{+/-}$ *Skp2*$^{-/-}$ and *Arf*$^{-/-}$ *Skp2*$^{-/-}$ MEFs, we next determined whether their upregulation contributes to senescence. *p27* (also known as *Cdkn1b*) shRNA efficiently abrogated p27 expression and partially rescued growth arrest and cellular senescence in *Pten*$^{+/-}$ *Skp2*$^{-/-}$ MEFs (Fig. 2c, d and Supplementary Figs 9a, b and 10a). Similarly, knockdown of *Atf4* or *p21* (also known as *Cdkn1a*) in these cells also partially reversed cellular senescence and cell arrest (Fig. 2e–h and Supplementary Figs 9c and 10b, c). Concomitant knockdown of *Atf4*, *p21* and *p27* in these cells reversed cellular senescence more efficiently than their individual knockdown (Supplementary Fig. 10d). In contrast, in *Skp2*$^{-/-}$ MEFs, *p27* knockdown accelerated growth whereas *Atf4* knockdown did not (Supplementary Fig. 10e, f). These results strongly indicate that the concomitant upregulation of p27, p21and Atf4 is a required and powerful engine for the induction of cellular senescence upon *Skp2* inactivation.

Skp2 loss restricts tumorigenesis independently of *Arf-p53*

We found that inactivation of *Skp2* in the presence of an oncogenic stress results in the induction of cellular senescence that opposes transformation *in vitro* even when the p19^{Arf}–p53 response is impaired. We next determined whether *Skp2* loss restricts tumorigenesis *in vivo* through similar mechanisms, and first analysed tumorigenesis in *Skp2*$^{-/-}$ *Pten*$^{+/-}$ compound mutants (Supplementary Fig. 11a). Although *Pten* heterozygous inactivation reduced lifespan in mice, compound *Skp2* deficiency prolonged overall survival (Fig. 3a). *Pten*$^{+/-}$ mice develop lymphadenopathy and adrenal tumours (pheochromacytoma) at complete penetrance[32,33]. As expected, *Pten*$^{+/-}$ mice developed adrenal tumours with 100% penetrance by 1 year of age, whereas *Skp2* loss remarkably abrogated adrenal tumour formation in compound mutants ($P < 0.0001$; Fig. 3b, top, c and Supplementary Fig. 11b). Pten protein expression in adrenal tissues was comparable between wild-type, *Pten*$^{+/-}$ and *Pten*$^{+/-}$ *Skp2*$^{-/-}$ mice, before or after tumour occurrence, suggesting that there is no loss of heterozygosity at the *Pten* locus in the adrenal tissues in any of these mutants and conditions (Supplementary Fig. 11c). Lymphadenopathy after *Pten* inactivation was also profoundly inhibited by *Skp2* loss ($P < 0.01$; Fig. 3b,

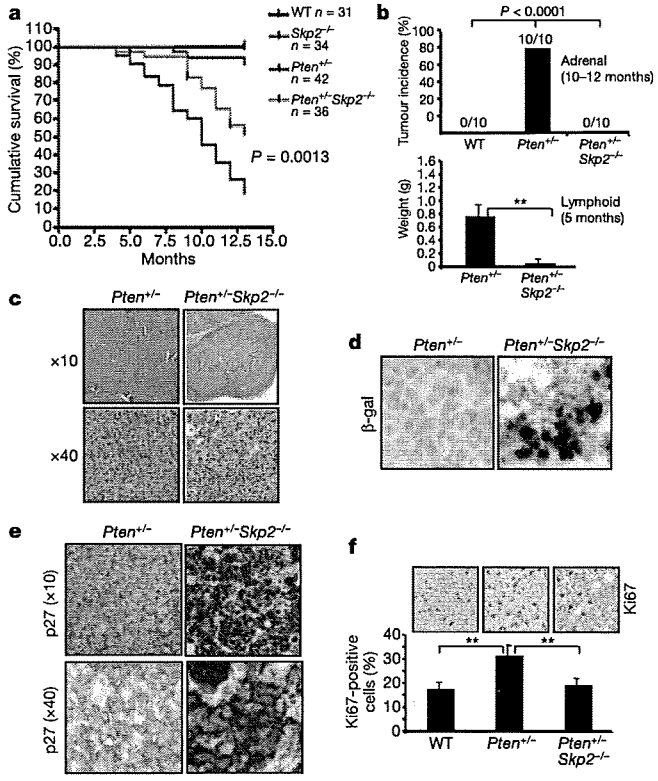

Figure 3 | *Skp2* deficiency restricts tumorigenesis after *Pten* inactivation by inducing cellular senescence *in vivo*. **a,** Kaplan–Meier plot analysis of cumulative survival of indicated mouse genotypes. **b,** Top, adrenal tissues from various mouse genotypes (10–12 months) were analysed for tumorigenesis; bottom, lymphoid tissues within the neck were obtained and weighed from female mice of various genotypes (around 5 months). **$P < 0.01$ using two-tailed Student's *t*-test, $n = 6$. **c,** Histological analysis of adrenal tissues from 12-month-old *Pten*$^{+/-}$ and *Pten*$^{+/-}$ *Skp2*$^{-/-}$ mice. *Pten*$^{+/-}$ mice developed adrenal tumour (pheochromocytoma), which was profoundly inhibited in *Pten*$^{+/-}$ *Skp2*$^{-/-}$ mice. **d,** Senescence analysis of lymphoid tissue from 5-month-old *Pten*$^{+/-}$ and *Pten*$^{+/-}$ *Skp2*$^{-/-}$ mice. **e,** Lymphoid tissues from 5-month-old mice of the indicated genotypes were obtained for p27 immunohistochemistry. **f,** Quantification of Ki67 staining of lymphoid tissues from 5-month-old mice. Results are mean ± s.d. **$P < 0.01$ using two-tailed Student's *t*-test, $n = 3$.

bottom and Supplementary Fig. 11d). Tumorigenesis was also markedly suppressed in other organs (for example, in the prostate, where the prostatic intraepithelial neoplasia (PIN) incidence was profoundly restricted by *Skp2* inactivation; data not shown).

To determine whether *Skp2* inactivation along with *Pten* inactivation would trigger cellular senescence *in vivo*, we performed SA-β-gal staining in the few hyperplastic lymphoid lesions still identified in $Pten^{+/-}$ $Skp2^{-/-}$ mice (see, for example, Supplementary Fig. 10d). We observed both cellular senescence and p27 induction in the lymphoid tissues from $Pten^{+/-}$ $Skp2^{-/-}$ mice (Fig. 3d, e and Supplementary Fig. 12), which inversely correlated with cell proliferation (Fig. 3f).

We then examined whether *Skp2* inactivation would also restrict tumorigenesis after *Arf* loss by crossing $Skp2^{-/-}$ with $Arf^{-/-}$ mice (Supplementary Fig. 13). *Skp2* inactivation markedly prolonged the overall survival of $Arf^{-/-}$ mice (Fig. 4a). Around 33% of $Arf^{-/-}$ mice developed sarcoma and/or lymphoma within 1 year (Fig. 4b–d)[34,35]. In contrast, none of the $Arf^{-/-}$ $Skp2^{-/-}$ compound mutant mice showed signs of tumour formation ($P < 0.02$; Fig. 4b–d).

Senescence after *Pten* and *Skp2* inactivation in the prostate

Complete *Pten* inactivation in the prostate triggers a tumour-suppressive cellular senescence response[2]. We therefore examined whether this response could be further potentiated by *Skp2* loss and affect tumorigenesis after complete *Pten* inactivation in the prostate. For prostate-specific inactivation, we made use of Cre-*loxP*-mediated recombination and probasin (*Pbsn*, also known as *PB*)-*Cre4* transgenic mice expressing the Cre recombinase after puberty in the prostatic epithelium[2]. We obtained $Pten^{loxP/loxP}$;*PB-Cre4* and $Pten^{loxP/loxP}Skp2^{-/-}$;*PB-Cre4* compound mutant mice, hereafter referred to as $Pten^{pc-/-}$ and $Pten^{pc-/-}$ $Skp2^{-/-}$ mice, respectively (Supplementary Fig. 14a). Although complete *Pten* inactivation in mouse prostates leads to invasive prostate cancers, it does not affect overall survival[2]. We did not detect a difference in overall survival between $Pten^{pc-/-}$ and $Pten^{pc-/-}$ $Skp2^{-/-}$ mice (Supplementary Fig. 14b).

Prostate cancer development in these mice was monitored by magnetic resonance imaging (MRI) and histopathological analysis. Consistent with our previous findings[2], MRI analysis showed prostate tumour masses in $Pten^{pc-/-}$ mice at 6 months of age, which were significantly reduced in $Pten^{pc-/-}$ $Skp2^{-/-}$ mice (Supplementary Fig. 14c). The average size of the prostate in $Pten^{pc-/-}$ mice was tenfold larger than in wild-type mice, whereas complete *Skp2* loss markedly reduced tumour weight after complete *Pten* inactivation (Fig. 5a). Histological analysis showed that *Skp2* loss inhibited invasive prostate cancer after *Pten* inactivation, albeit PIN lesions were still observed in $Pten^{pc-/-}$ $Skp2^{-/-}$ mice (Supplementary Fig. 14d, e). Furthermore, this suppressive effect by *Skp2* loss was persistent, as we also observed a profound reduction in tumour weight and invasive prostate cancer in $Pten^{pc-/-}$ $Skp2^{-/-}$ mice at 15 months of age (Supplementary Fig. 14f, g).

We next investigated, *in vivo*, the molecular basis for tumour suppression elicited by Skp2 inactivation. We found that p27 protein expression was synergistically induced in prostates from compound mutants, as determined by immunohistochemistry and western blot analysis (Supplementary Fig. 15a, b), whereas p53 expression was comparably induced in $Pten^{pc-/-}$ and $Pten^{pc-/-}$ $Skp2^{-/-}$ mice

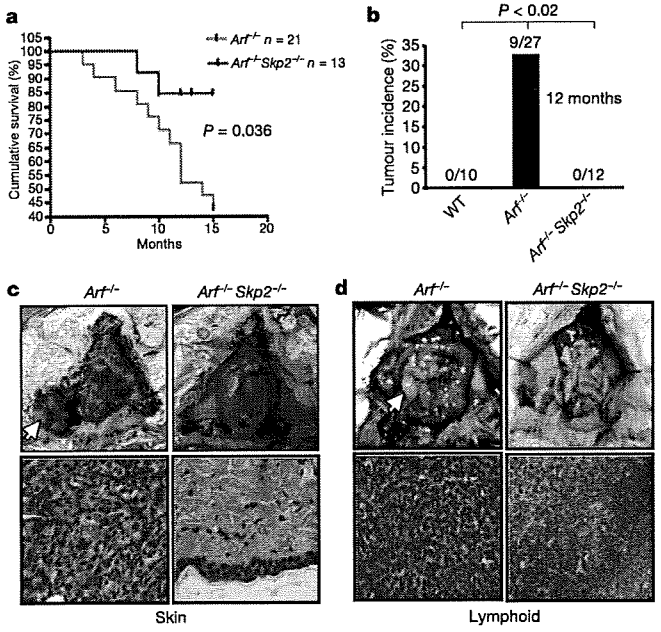

Figure 4 | *Skp2* inactivation restricts tumorigenesis upon *Arf* deficiency. **a**, Kaplan–Meier plot analysis of cumulative survival of $Arf^{-/-}$ and $Arf^{-/-}$ $Skp2^{-/-}$ mice. **b**, A cohort of wild-type, $Arf^{-/-}$ and $Arf^{-/-}$ $Skp2^{-/-}$ mice were analysed for tumorigenesis within a 1-year period. $Arf^{-/-}$ $Skp2^{-/-}$ mice did not develop any tumour up to 1 year observation. Nine out of twenty-seven $Arf^{-/-}$ mice developed either sarcoma or lymphomas, whereas none of 12 $Arf^{-/-}$ $Skp2^{-/-}$ mice developed tumours. The statistic was analysed by chi-squared test, χ^2. **c**, Histopathological analysis of skin tissues from $Arf^{-/-}$ and $Arf^{-/-}$ $Skp2^{-/-}$ mice at 1 year old. Arrow indicates sarcoma. **d**, Histopathological analysis of lymphoid tissues lymphoid tissues from $Arf^{-/-}$ and $Arf^{-/-}$ $Skp2^{-/-}$ mice at 1 year of age. The arrow indicates lymphoma. Original magnification, ×40 (**c**, **d**).

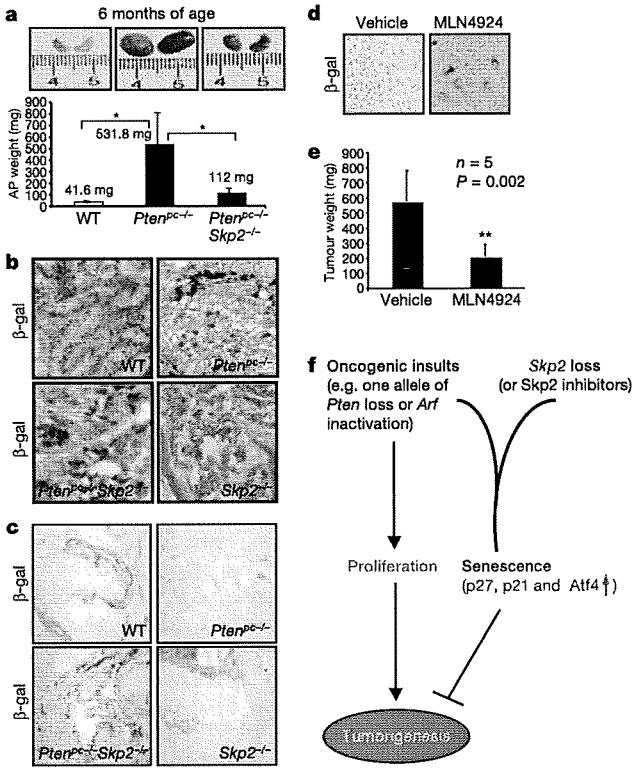

Figure 5 | *Skp2* deficiency restricts prostate cancer development by triggering cellular senescence *in vivo*. **a**, Biopsy of anterior prostate (AP) tumours at 24 weeks from various genotypes of mice and their actual sizes and weights. Results are mean ± s.d. $^*P < 0.05$ using two-tailed Student's *t*-test, $n = 5$. **b**, **c**, Senescence analysis of anterior prostate from $Pten^{pc-/-}$ and $Pten^{pc-/-}$ $Skp2^{-/-}$ mice aged 3 months (**b**) or 15 months (**c**). A representative section from three mice is presented for each genotype. Original magnifications, ×40 (**b**) and ×20 (**c**). **d**, PC3 cells were treated with vehicle or 0.1 μM MLN4924 for 4 days and collected for cellular senescence assay. **e**, Nude mice bearing PC3 xenograft tumours (around 300 mm^3) were treated with vehicle or MLN492, and tumour weight was measured. **f**, Working model for tumour-suppressive cellular senescence driven by oncogenic insults and *Skp2* deficiency.

(Supplementary Fig. 15c). *Skp2* deficiency profoundly enhanced cellular senescence upon *Pten* inactivation (Fig. 5b). This was observed at earlier time points and inversely correlated with cell proliferation (Supplementary Fig. 16a, b). Notably, this response was also sustained over time. We could detect massive β-gal positivity in prostates from $Pten^{pc-/-}$ $Skp2^{-/-}$ mice even at 15 months of age, whereas β-gal positivity was barely detected at that age in prostates from $Pten^{pc-/-}$ mice (Fig. 5c). Thus, *Skp2* inactivation potentiates and sustains over time the senescence response elicited by an oncogenic stimulus, suggesting that pharmacological inhibition of Skp2 may be used as a powerful pro-senescence approach for cancer therapy and chemoprevention.

Skp2–SCF complex inactivation triggers senescence

To corroborate the potential use of such an approach for cancer therapy, we determined whether pharmacological inactivation of the Skp2–SCF complex induces cellular senescence in p53-deficient cells and, importantly, suppresses the growth of the pre-formed tumours. To this end, we took advantage of MLN4924 (ref. 36)—an inhibitor for the neddylation of cullin 1, which is a component of Skp2–SCF complex. We used PC3 prostate cancer cells for this preclinical analysis because these cells are both p53-null and Pten-null, hence representing one of the most aggressive genetic states encountered in human cancer. Remarkably, treatment of MLN4924 in PC3 cells triggered cellular senescence (Fig. 5d). Moreover, the growth of PC3 tumours treated with MLN4924 *in vivo* was also suppressed (Fig. 5e). Coherent with these findings, *Skp2* silencing in PC3 and in DU145 prostate cancer cells, which have also evaded the p53 response, triggered cellular senescence and cooperated with the DNA-damaging agent doxorubicin to induce cellular senescence and growth arrest (Supplementary Fig. 17). These results demonstrate the critical role of Skp2 inactivation in the induction of cellular senescence not only in mouse cells, but also in human cancer cells experiencing failure of p53 and other major tumour-suppressive networks.

Discussion

On the basis of our results, we propose a working model for the role of *Skp2* inactivation-induced cellular senescence in tumour prevention and suppression *in vivo* (Fig. 5f). This model rests on three new and unexpected findings with important therapeutic implications. First, *Skp2* inactivation does not trigger cellular senescence *in vivo* or *in vitro* on its own, but rather elicits a senescence response after oncogenic stress. This response is critically dependent on p27, p21 and Atf4 induction. Our results are supported by recent reports showing that acute inactivation of the von Hippel–Lindau (VHL) tumour suppressor *in vitro* or overexpression of the human T-lymphotropic virus type 1 (HTLV-1) Tax triggers Skp2 downregulation and cellular senescence[37,38]. Second, we show that cellular senescence driven by *Skp2* inactivation along with oncogenic insults takes place without the activation of the $p19^{Arf}$–p53 failsafe pathway. Although senescence is also observed in p53/Pten-null cells such as PC3, it will be important to determine the specific genetic states that favour evasion of this failsafe mechanism, also in a cell-type-specific manner. For instance, loss or constitutively low expression of p27, p21 and Atf4 could impair this response. This knowledge will in turn identify new pharmacological nodes of tumour-type-specific intervention. Third, we show that *Skp2* deficiency in conjunction with oncogenic signals elicits a senescence response that profoundly restricts tumorigenesis *in vivo* in numerous mouse models in which tumour suppressor networks are faulty or inactive. Our findings are consistent with a recent report demonstrating that mice transplanted with BCR–ABL-transduced $Skp2^{-/-}$ bone marrow cells show a delayed onset of a myeloproliferative syndrome[39].

As Skp2 can in principle be subjected to specific pharmacological inhibition because of its enzymatic activity, our results call for the development and optimization of Skp2 small molecule inhibitors. Skp2 pharmacological inhibition could be particularly appealing and effective in view of the fact that complete Skp2 inactivation in the mouse is compatible with life, whereas cellular senescence is only triggered by Skp2 inactivation in conjunction with oncogenic conditions.

METHODS SUMMARY

$Pten^{loxP/loxP}$, $Arf^{-/-}$ and $Skp2^{-/-}$ mice were generated as described previously[2,18,35]. Female $Pten^{loxP/loxP}$ mice were crossed with male *PB-Cre4* transgenic mice for the prostate-specific deletion of *Pten*. MEFs from wild-type and $Skp2^{-/-}$ mice were prepared as previously described[40,41] and cultured in DMEM containing 10% FBS. Cellular senescence was determined by assessing SA-β-gal activity, and the *in vivo* cell proliferation assay was performed by Ki67 staining on the paraffin tissue sections. The cell transformation assay was determined by the soft agar assay. *p53* shRNA is from S. W. Lowe and the pBabe-p53 dominant-negative construct is a gift from M. Oren. MLN4924 was obtained from Millennium Pharmaceuticals.

Full Methods and any associated references are available in the online version of the paper at www.nature.com/nature.

Received 9 October 2009; accepted 11 January 2010.

1. Sharpless, N. E. & DePinho, R. A. Cancer: crime and punishment. *Nature* **436**, 636–637 (2005).
2. Chen, Z. *et al.* Crucial role of p53-dependent cellular senescence in suppression of Pten-deficient tumorigenesis. *Nature* **436**, 725–730 (2005).
3. Xue, W. *et al.* Senescence and tumour clearance is triggered by p53 restoration in murine liver carcinomas. *Nature* **445**, 656–660 (2007).
4. Ventura, A. *et al.* Restoration of p53 function leads to tumour regression *in vivo*. *Nature* **445**, 661–665 (2007).
5. Braig, M. *et al.* Oncogene-induced senescence as an initial barrier in lymphoma development. *Nature* **436**, 660–665 (2005).
6. Michaloglou, C. *et al.* BRAFE600-associated senescence-like cell cycle arrest of human naevi. *Nature* **436**, 720–724 (2005).
7. Collado, M. *et al.* Tumour biology: senescence in premalignant tumours. *Nature* **436**, 642 (2005).
8. Cantley, L. C. & Neel, B. G. New insights into tumor suppression: PTEN suppresses tumor formation by restraining the phosphoinositide 3-kinase/AKT pathway. *Proc. Natl Acad. Sci. USA* **96**, 4240–4245 (1999).
9. Di Cristofano, A. & Pandolfi, P. P. The multiple roles of PTEN in tumor suppression. *Cell* **100**, 387–390 (2000).
10. Salmena, L., Carracedo, A. & Pandolfi, P. P. Tenets of PTEN tumor suppression. *Cell* **133**, 403–414 (2008).
11. Bloom, J. & Pagano, M. Deregulated degradation of the cdk inhibitor p27 and malignant transformation. *Semin. Cancer Biol.* **13**, 41–47 (2003).
12. Nakayama, K. I. & Nakayama, K. Regulation of the cell cycle by SCF-type ubiquitin ligases. *Semin. Cell Dev. Biol.* **16**, 323–333 (2005).
13. Gstaiger, M. *et al.* Skp2 is oncogenic and overexpressed in human cancers. *Proc. Natl Acad. Sci. USA* **98**, 5043–5048 (2001).
14. Latres, E. *et al.* Role of the F-box protein Skp2 in lymphomagenesis. *Proc. Natl Acad. Sci. USA* **98**, 2515–2520 (2001).
15. Shim, E. H. *et al.* Expression of the F-box protein SKP2 induces hyperplasia, dysplasia, and low-grade carcinoma in the mouse prostate. *Cancer Res.* **63**, 1583–1588 (2003).
16. Lin, H. K. *et al.* Phosphorylation-dependent regulation of cytosolic localization and oncogenic function of Skp2 by Akt/PKB. *Nature Cell Biol.* **11**, 420–432 (2009).
17. Chiarle, R. *et al.* S-phase kinase-associated protein 2 expression in non-Hodgkin's lymphoma inversely correlates with p27 expression and defines cells in S phase. *Am. J. Pathol.* **160**, 1457–1466 (2002).
18. Nakayama, K. *et al.* Targeted disruption of *Skp2* results in accumulation of cyclin E and $p27^{Kip1}$, polyploidy and centrosome overduplication. *EMBO J.* **19**, 2069–2081 (2000).
19. Lin, A. W. *et al.* Premature senescence involving p53 and p16 is activated in response to constitutive MEK/MAPK mitogenic signaling. *Genes Dev.* **12**, 3008–3019 (1998).
20. Serrano, M., Lin, A. W., McCurrach, M. E., Beach, D. & Lowe, S. W. Oncogenic *ras* provokes premature cell senescence associated with accumulation of p53 and $p16^{INK4a}$. *Cell* **88**, 593–602 (1997).
21. Kim, W. Y. & Sharpless, N. E. The regulation of INK4/ARF in cancer and aging. *Cell* **127**, 265–275 (2006).
22. Yaswen, P. & Campisi, J. Oncogene-induced senescence pathways weave an intricate tapestry. *Cell* **128**, 233–234 (2007).
23. Hemann, M. T. *et al.* An epi-allelic series of p53 hypomorphs created by stable RNAi produces distinct tumor phenotypes *in vivo*. *Nature Genet.* **33**, 396–400 (2003).
24. Gottlieb, E., Haffner, R., von Ruden, T., Wagner, E. F. & Oren, M. Down-regulation of wild-type p53 activity interferes with apoptosis of IL-3-dependent hematopoietic cells following IL-3 withdrawal. *EMBO J.* **13**, 1368–1374 (1994).
25. Chen, Z. *et al.* Differential p53-independent outcomes of $p19^{Arf}$ loss in oncogenesis. *Sci. Signal.* **2**, ra44 (2009).
26. Bartkova, J. *et al.* Oncogene-induced senescence is part of the tumorigenesis barrier imposed by DNA damage checkpoints. *Nature* **444**, 633–637 (2006).

27. Di Micco, R. *et al.* Oncogene-induced senescence is a DNA damage response triggered by DNA hyper-replication. *Nature* **444**, 638–642 (2006).
28. Mallette, F. A., Gaumont-Leclerc, M. F. & Ferbeyre, G. The DNA damage signaling pathway is a critical mediator of oncogene-induced senescence. *Genes Dev.* **21**, 43–48 (2007).
29. Yu, Z. K., Gervais, J. L. & Zhang, H. Human CUL-1 associates with the SKP1/SKP2 complex and regulates $p21^{CIP1/WAF1}$ and cyclin D proteins. *Proc. Natl Acad. Sci. USA* **95**, 11324–11329 (1998).
30. Denoyelle, C. *et al.* Anti-oncogenic role of the endoplasmic reticulum differentially activated by mutations in the MAPK pathway. *Nature Cell Biol.* **8**, 1053–1063 (2006).
31. Kim, I., Xu, W. & Reed, J. C. Cell death and endoplasmic reticulum stress: disease relevance and therapeutic opportunities. *Nature Rev. Drug Discov.* **7**, 1013–1030 (2008).
32. Di Cristofano, A. *et al.* Impaired Fas response and autoimmunity in $Pten^{+/-}$ mice. *Science* **285**, 2122–2125 (1999).
33. Di Cristofano, A., Pesce, B., Cordon-Cardo, C. & Pandolfi, P. P. Pten is essential for embryonic development and tumour suppression. *Nature Genet.* **19**, 348–355 (1998).
34. Kamijo, T., Bodner, S., van de Kamp, E., Randle, D. H. & Sherr, C. J. Tumor spectrum in ARF-deficient mice. *Cancer Res.* **59**, 2217–2222 (1999).
35. Kamijo, T. *et al.* Tumor suppression at the mouse *INK4a* locus mediated by the alternative reading frame product $p19^{ARF}$. *Cell* **91**, 649–659 (1997).
36. Soucy, T. A. *et al.* An inhibitor of NEDD8-activating enzyme as a new approach to treat cancer. *Nature* **458**, 732–736 (2009).
37. Young, A. P. *et al.* VHL loss actuates a HIF-independent senescence programme mediated by Rb and p400. *Nature Cell Biol.* **10**, 361–369 (2008).
38. Kuo, Y. L. & Giam, C. Z. Activation of the anaphase promoting complex by HTLV-1 tax leads to senescence. *EMBO J.* **25**, 1741–1752 (2006).
39. Agarwal, A. *et al.* Absence of SKP2 expression attenuates BCR-ABL-induced myeloproliferative disease. *Blood* **112**, 1960–1970 (2008).
40. Lin, H. K., Bergmann, S. & Pandolfi, P. P. Cytoplasmic PML function in TGF-β signalling. *Nature* **431**, 205–211 (2004).
41. Yang, W. L. *et al.* The E3 ligase TRAF6 regulates Akt ubiquitination and activation. *Science* **325**, 1134–1138 (2009).

Supplementary Information is linked to the online version of the paper at www.nature.com/nature.

Acknowledgements We are grateful to C. J. Sherr, S. W. Lowe and M. Oren for mice and reagents. We would also like to thank B. Carver, L. DiSantis, J. Clossey and S. Megan for editing and critical reading of the manuscript, J. A. Koutcher, C. Le, C. Matei and M. Lupa for MRI analysis, as well all the members of the Pandolfi laboratory for comments and discussion. We extend our thanks to M. Rolfe, P. G. Smith, and Millennium Pharmaceuticals for discussion and for providing the MLN4924 compound. This work was supported by NIH grants to P.P.P. and M.D. Anderson Trust Scholar Award and DOD Prostate Cancer New Investigator Award to H.K.L.

Author Contributions H.K.L. and P.P.P. designed the experiments and wrote the manuscript; H.-K.L., Z.C., G.W., S.-W.L., C.N., C.-H.C., W.-L.Y., J.W. and A.E. performed the experiments; C.C.-C. and J.T-F. performed the histopathological analysis of the mice; K.I.N. provided the $Skp2^{-/-}$ mice.

Author Information Reprints and permissions information is available at www.nature.com/reprints. The authors declare no competing financial interests. Correspondence and requests for materials should be addressed to P.P.P. (ppandolf@bidmc.harvard.edu).

METHODS

shRNA-mediated silencing. For the retrovirus-infection system, *p27* shRNA (5′-GTGGAATTTCGACTTTCAG-3′), *Atf4* shRNA (5′-GAGCATTCCTTTAG TTTAG-3′), and GFP shRNA (5′-GCAAGCTGACCCTGAAGTTC-3′) were subcloned into the pSUPER-puro vector (Oligoengine) according to standard procedures and transfected into Phoenix packaging cells. For lentiviral shRNA infection, 293T cells were co-transfected with *p27*, *Atf4*, *p21*, *Skp2* or GFP control shRNA along with packing plasmids (ΔVPR8.9) and envelope plasmid (VSV-G) using Lipofectamine 2000 reagents according to the manufacturer's instructions. *Skp2*-lentivivral shRNA-1 (5′-GATAGTGTCATGCTAAAGAAT-3′), *p27*-lentivivral shRNA-1 (5′-CGCAAGTGGAATTTCGACTTT-3′), *p27*-lentivivral shRNA-2 (5′-CCCGGTCAATCATGAAGAACT-3′), *Atf4*-lentivivral shRNA-1 (5′-GCGAG TGTAAGGAGCTAGAAA-3′), *Atf4*-lentivivral shRNA-2 (5′-CGGACAAAGATA CCTTCGAGT-3′), *p21*-lentivivral shRNA-1 (5′ CTGGTGTCTGAGCGGCCT GAA-3′), *p21*-lentivivral shRNA-2 (5′-GACAGATTTCTATCACTCCAA-3′), and GFP shRNA (5′-GCAAGCTGACCCTGAAGTTC-3′) were transfected with packing plasmids into 293T cells for 2 days, and virus particles containing *p27*, *p21*, *Atf4*, *Skp2* or GFP shRNA were used to infect mammalian cells. All the infected cells were cultured in a medium containing the appropriate antibiotics.

Western blot analysis and immunohistochemistry. Cell lysates were prepared with RIPA buffer (PBS, 1% Nonidet P40, 0.5% sodium deoxycholate, 0.1% SDS and protease inhibitor cocktail (Roche)). The following antibodies were used for western blot analysis: anti-$p19^{Arf}$ (NeoMarkers), anti-p53 (Novocastra), anti-p21 (Santa Cruz), anti-β-actin (Sigma), anti-Hsp90 (BD transduction laboratories), anti-p27 (BD transduction laboratories), anti-α-tubulin (Sigma), anti-phospho-p53 (Ser15) (Cell Signaling), anti-phospho-H2ax (Ser139) (Cell Signaling), anti-phospho-eIF2α (Ser51) (Cell Signaling), anti-eIF2α (Cell Signaling), anti-phospho-Perk (Thr980) (Cell Signaling), anti-cyclin D1 (Santa Cruz), anti-E2F1 (Santa Cruz), anti-Cdt1 (Proteintech Group), anti-Ras (Oncogene), anti-E1A (Neomarkers), and anti-Atf4 (Santa Cruz). For immunohistochemistry, tissues were fixed in 10% formalin and embedded in paraffin in accordance with standard procedures. Sections were stained with anti-p27 (BD transduction laboratories), anti-Ki67 (Novocastra), anti-Pten (Neomarkers) and anti-p53 (Novocastra) antibodies.

Cell proliferation, transformation and senescence. Primary MEFs were isolated from individual embryos of various genotype at passage 2, infected with retroviruses or lentiviruses expressing GFP shRNA, *p27* shRNA or *Atf4* shRNA for 2 days, selected with 2 $\mu g\,ml^{-1}$ puromycin for 4 days, and plated for the cell proliferation and senescence assay. For cell proliferation assay, 2×10^4 MEFs were seeded in 12 wells in triplicate, collected, and stained with trypan blue at different days. Numbers of viable cells were directly counted under the microscope. To determine cellular senescence, MEFs were plated at 10^4 cells per well of a 6-well plate in triplicate, and after 4 days SA-β-gal activity was measured using the senescence detection kit (Calbiochem) and quantified (around 100–200 cells per well). For *in vivo* cellular senescence, frozen sections 6-μm thick were stained for β-gal as described earlier. For *in vivo* cell proliferation, the paraffin section was used for Ki67 staining, and the percentages of Ki67-positive cells (around 500 cells) from each sample were counted. For transformation assay, wild-type and $Skp2^{-/-}$ MEFs (3×10^4) infected with Ras(G12V) and E1A were suspended in a medium containing 0.3% agar onto solidified 0.6% agar per well of a 6-well plate, and the number of colonies was counted after 21 days.

Apoptosis assay. Primary MEFs of various genotypes of mouse embryos were cultured in 10% FBS for 2 days; cells were collected and labelled with Annexin-V–FITC, followed by a flow cytometry analysis.

MRI. Individual mice were subjected to MRI assessment for the detection of prostate tumours as described[42].

***In vivo* drug treatment in the preclinical tumour model.** Nude mice bearing PC3 xenograft tumours (around 300 mm^3) were treated with vehicle or 90 $mg\,kg^{-1}$ MLN492. Tumour weight was measured at the time of collection after 15 days of treatment with a scheduling regimen of 3 days of treatment followed by 3 days without treatment for a total of three courses.

42. Chen, Z. *et al.* Crucial role of p53-dependent cellular senescence in suppression of Pten-deficient tumorigenesis. *Nature* **436**, 725–730 (2005).

JOURNAL OF VIROLOGY, Jan. 2010, p. 822–832 Vol. 84, No. 2
0022-538X/10/$12.00 doi:10.1128/JVI.01339-09

Extrachromosomal Histone H2B Mediates Innate Antiviral Immune Responses Induced by Intracellular Double-Stranded DNA▽†

Kouji Kobiyama,[1,4]‡ Fumihiko Takeshita,[1]‡* Nao Jounai,[1] Asako Sakaue-Sawano,[2] Atsushi Miyawaki,[2] Ken J. Ishii,[3,4] Taro Kawai,[3] Shin Sasaki,[1] Hisashi Hirano,[5] Norihisa Ishii,[6] Kenji Okuda,[1] and Koichi Suzuki[6]‡*

Department of Molecular Biodefense Research, Yokohama City University Graduate School of Medicine, Yokohama 236-0004, Japan[1]; Laboratory for Cell Function Dynamics, Advanced Technology Development Group, Brain Science Institute, RIKEN, Wako 351-0198, Japan[2]; Laboratory of Host Defense, WPI Immunology Frontier Research Center, Osaka University, Suita 565-8701, Japan[3]; Department of Molecular Protozoology, Research Institute for Microbial Diseases, Osaka University, Suita 565-8701, Japan[4]; International Graduate School of Arts and Sciences, Yokohama City University, Yokohama 230-0045, Japan[5]; and Department of Bioregulation, National Institute of Infectious Diseases, Higashimurayama-shi 189-0002, Japan[6]

Received 29 June 2009/Accepted 2 November 2009

Fragments of double-stranded DNA (dsDNA) forming a right-handed helical structure (B-DNA) stimulate cells to produce type I interferons (IFNs). While an adaptor molecule, IFN-β promoter stimulator 1 (IPS-1), mediates dsDNA-induced cellular signaling in human cells, the underlying molecular mechanism is not fully understood. Here, we demonstrate that the extrachromosomal histone H2B mediates innate antiviral immune responses in human cells. H2B physically interacts with IPS-1 through the association with a newly identified adaptor, CIAO (*C*OOH-terminal *i*mportin 9-related *a*daptor *o*rganizing histone H2B and IPS-1), to transmit the cellular signaling for dsDNA but not immunostimulatory RNA. Extrachromosomal histone H2B was biologically crucial for cell-autonomous responses to protect against multiplication of DNA viruses but not an RNA virus. Thus, the present findings provide evidence indicating that the extrachromosomal histone H2B is engaged in the signaling pathway initiated by dsDNA to trigger antiviral innate immune responses.

Fragments of nucleic acids derived from either infectious agents or host cells activate cell-autonomous responses to inhibit multiplication of certain viruses by inducing type I interferon (IFN) production (5). Such effects are more evident when double-stranded DNA (dsDNA) is transduced into the intracellular compartment by use of a transfection agent or electroporation method, suggesting that the DNA sensing system recognizes aberrant DNA fragments inside the cell (6, 21, 23). dsDNA forming a right-handed helical structure, i.e., B-DNA, has a greater ability to induce type I IFNs than Z-DNA, which has a left-handed zig-zag structure (6). dsDNA activates type I IFN production in a wide variety of cell types, including immune cells, such as dendritic cells and macrophages, and nonimmune cells, such as fibroblasts, epithelial cells, and thyroid cells (6, 23). Such effects of dsDNA were corroborated by the observation in mice deficient for DNase II, in which intracellular accumulation of undegraded DNA fragments resulted in hyperproduction of IFN-β, dysregulation of erythropoiesis, and symptoms resembling rheumatoid arthritis (12, 28). The loss-of-function mutation of the *DNase I* gene has been found in patients with systemic lupus erythematosus (SLE) and, in fact, *DNase* $I^{-/-}$ mice manifest SLE-like symptoms with anti-DNA antibody (Ab) production (18, 27).

The immunostimulatory property of dsDNA is quite similar to that of immunostimulatory RNA (isRNA), such as dsRNA and 5′-triphosphate RNA (2, 6). Indeed, the signaling pathways engaged by dsDNA in part are shared with those for isRNA. Retinoic acid-inducible gene I (RIG-I) and melanoma differentiation-associated gene 5 (MDA5) directly associate with isRNA and trigger signaling, while it has been demonstrated that RIG-I does not directly interact with dsDNA but mediates its signaling in a human hepatoma cell line, Huh7 (2). IFN-β promoter stimulator 1 (IPS-1, also known as mitochondrial antiviral signaling), mediates the downstream signaling induced by dsDNA or isRNA in humans, while IPS-1 solely mediates isRNA but not dsDNA signaling in mice (2, 6, 15, 22). In contrast, TANK-binding kinase 1 (TBK1) and inducible IκB kinase (IKKi) are essential for dsDNA- or isRNA-induced type I IFN production in both humans and mice (2, 6). While examining distinct molecules involved in dsDNA-mediated but not isRNA-mediated upstream signaling, Z-DNA binding protein 1 (ZBP1, also known as DNA-dependent activator of IFN regulatory factors [DAI]) was identified as a candidate cytosolic DNA sensor, at least in a mouse connective tissue cell line, L929, although its *in vivo* role was dispensable (7, 24, 26). Recently, a PYHIN family member, Absent in melanoma 2

* Corresponding author. Mailing address for Fumihiko Takeshita: Department of Molecular Biodefense Research, Yokohama City University Graduate School of Medicine, 3-9 Fukuura, Kanazawaku, Yokohama 236-0004, Japan. Phone: 81-45-787-2602. Fax: 81-45-787-2851. E-mail: takesita@yokohama-cu.ac.jp. Mailing address for Koichi Suzuki: Department of Bioregulation, Leprosy Research Center, National Institute of Infectious Diseases, 4-2-1 Aoba-cho, Higashimurayama-shi, Tokyo 189-0002, Japan. Phone: 81-42-391-8211. Fax: 81-42-394-9092. E-mail: koichis@nih.go.jp.

† Supplemental material for this article may be found at http://jvi.asm.org/.

‡ K.K., F.T., and K.S. contributed equally to this work.

▽ Published ahead of print on 11 November 2009.

(AIM2) protein, was shown to associate with an inflammasome signaling adaptor, apoptosis-associated speck-like protein containing a CARD (ASC), and to play a critical role for caspase 1 activation and interleukin-1β (IL-1β) secretion in response to dsDNA (1, 3, 4, 20).

In the present study, we show that extrachromosomal histone H2B is responsible for the dsDNA-induced type I IFN production in human cells and for the innate immune response to DNA virus infection.

MATERIALS AND METHODS

Cells and reagents. HEK293T, HEK293, HeLa, NIH 3T3, Vero, and L929 cells were purchased from the American Type Culture Collection (Manassas, VA) and maintained in Dulbecco's modified Eagle's medium supplemented with 10% fetal calf serum and 50 μg/ml penicillin-streptomycin. SCC-4 squamous carcinoma cells (JCRB9118) were obtained from Human Science Research Resources Bank (Osaka, Japan). Human umbilical vein endothelial cells (HUVEC) were obtained from Cambrex BioScience (Waikersville, MD). IPS-$1^{-/-}$ murine embryonic fibroblasts (MEF) were previously described (15). Encephalomyocarditis virus (EMCV) and mouse cytomegalovirus (MCMV) strain MW97.01 were kindly provided by T. Fujita (Kyoto University, Kyoto, Japan) and U. H. Koszinowski (Max von Pettenkofer Institute for Virology, Munich, Germany), respectively. poly(dA·dT)·poly(dA·dT) [designated poly(dA·dT)] and poly(dG·dC)·poly(dG·dC) [designated poly(dC·dG)] were purchased from Amersham Biosciences (Piscataway, NJ). Poly(I:C) and human tumor necrosis factor alpha (TNF-α) were obtained from Invivogen (San Diego, CA) and PeproTech EC (London, United Kingdom), respectively. MVAdE3L was a kind gift from Holger Ludwig (Paul-Ehrlich Institute, Langen, Germany). The human papillomavirus (HPV) genome cloned in pBR322 (pHPV11) was obtained from JCRB GenBank (Osaka, Japan). Each nucleic acid was mixed for 15 min with *Trans*IT-LT1 (Mirus Bio, Madison, WI) or Lipofectamine 2000 reagent (Invitrogen) at a constant weight/volume ratio of 1:3 in serum-free medium before use for stimulation.

Screening of the cDNA expression library. A cDNA expression library originated from human bone marrow (Invitrogen) was screened. *Escherichia coli* DH5α cells transformed with a human bone marrow cDNA library (Invitrogen) were subdivided into ~20 independent clones or 4,800 pools. Each pool was cultured at 30°C for 48 h, and then library plasmid DNA was extracted using the Wizard SV 96 plasmid DNA purification system (Promega, Madison, WI). HEK293T cells stably transfected with pGL3 IFN-β were transiently transfected with each pool of the library plasmids using FuGENE6 transfection reagent. Twenty-four hours after transfection, cells were washed and then stimulated with 0.5 μg/ml of poly(dA·dT). Luciferase assays were performed using the Bright-Glo luciferase assay system 24 h after stimulation. The three pools that showed the highest luciferase activities were transformed into DH5α, and then library plasmid DNA from 50 independent clones was recovered. A second screening was performed using these single plasmids in the same manner. Finally, insert cDNA from selected clones was sequenced using a Genetic Analyzer 310 apparatus (PE Applied Biosystems, Foster City, CA) and then characterized with the BLAST program.

RNA interference. Interference of histone mRNA was performed as described previously (6). dsRNA was chemically synthesized by Invitrogen (stealth RNAi; Carlsbad, CA) or iGENE (Hokkaido, Japan). Sequences of each RNA were as follows: histone H1 sense, 5′-GCC CAA GAA AGU AGC UAA AAG CCC UAG-3′; histone H1 antisense, 5′-AGG GCU UUU AGC UAC UUU CUU GGG CAU-3′; histone H2A sense, 5′-CGC AAC GAC GAG GAA CUG AAC AAG CAG-3′; histone H2A antisense, 5′-GCU UGU UCA GUU CCU CGU CGU UGC GAU-3′; histone H2Bf116 sense, 5′-CCG UUU ACG UGU ACA AGG UGC UGA A-3′; histone H2Bf116 antisense, 5′-UUC AGC ACC UUG UAC ACG UAA ACG G-3′; histone H2Bf169 sense, 5′-UCC AAG GCC AUG GGC AUC AUG AAC U-3′; histone H2Bf169 antisense, 5′-AGU UCA UGA UGC CCA UGG CCU UGG A-3′; histone H3 sense, 5′-GAG AUC GCU CAG GAC UUU AAG ACC GAG-3′; histone H3 antisense, 5′-CGG UCU UAA AGU CCU GAG CGA UCU CAU-3′; histone H4 sense, 5′-GGG ACA AUA UCC AAG GCA UUA CAA AAG-3′; histone H4 antisense, 5′-UUU GUA AUG CCU UGG AUA UUG UCC CAU-3′; CIAO sense, 5′-AUG GAC AGU AUG AAG GCA AAG UCA GAG-3′; CIAO antisense, 5′-CUG ACU UUG CCU UCA UAC UGU CCA UAU-3′; ZBP1A sense, 5′-AUU UCA UGU GGA UUC UCU GGG CGG C-3′; ZBP1A antisense, 5′-GCC GCC CAG AGA AUC CAC AUG AAA U-3′; ZBP1B sense, 5′-UGU UGC UGU UGC CGA UGG UGG CGU C-3′; ZBP1B antisense, 5′-GAC GCC ACC AUC GGC AAC AGC AAC A-3′; ZBP1C sense, 5′-UUC AUC CAC AUA GUG GCU GCC UUC U-3′; ZBP1C antisense, 5′-AGA AGG CAG CCA CUA UGU GGA UGA A-3′; RIG-IA sense, 5′-UUA GGA UUC UCA UUG CUG GGA UCC C-3′; RIG-IA antisense, 5′-GGG AUC CCA GCA AUG AGA AUC CUA A-3′; RIG-IB sense, 5′-AUG UCU UGU ACU UCA CAU GGA UUC C-3′; RIG-IB antisense, 5′-GGA AUC CAU GUG AAG UAC AAG ACA U-3′; RIG-IC sense, 5′-UGG ACA UGA AUU CUC ACU AAG AUU C-3′; RIG-IC antisense, 5′-GAA UCU UAG UGA GAA UUC AUG UCC A-3′. The cells (6×10^5) were transfected with 120 pmol of each dsRNA by using the Lipofectamine RNAi MAX reagent (Invitrogen) according to the manufacturer's protocol.

Generation of mammalian expression plasmids. H2B, RIG-I, ZBP1, TBK1, and CIAO cDNA was amplified by PCR using a human or mouse spleen cDNA library or the isolated library plasmid as a template. cDNA fragments were verified by sequencing and then introduced into pFLAG-CMV4 (Sigma), pFLAG-CMV5 (Sigma), or pCIneo-HA (25), or pCAGGS-CFP, pCAGGS-YFP, or pcDNA3-mRFP (10). To obtain full-length and truncated mutants of CIAO, the full-length CIAO open reading frame (ORF; amino acids [aa] 1 to 249), aa 1 to 121, aa 91 to 249, or aa 194 to 249 was fused to the green fluorescent protein (GFP) ORF and introduced into pFLAG-CMV4 (FLAG-CIAO FL-GFP, FLAG-CIAO N′-3a-GFP, FLAG-CIAO C′-4a-GFP, or FLAG-CIAO C′-2a-GFP, respectively). To obtain a truncated mutant of histone H2B, the full-length histone H2B ORF (aa 1 to 126), aa 1 to 103, aa 1 to 86, aa 1 to 53, or aa 1 to 37 (nuclear localization signal), or aa 38 to 126 (α-helical region) was fused to the GFP ORF and introduced into pCIneo-HA [HA-H2B FL (N′-1α2α3α4α)-GFP, HA-H2B N′-1α2α3α-GFP, HA-H2B N′-1α2α-GFP, HA-H2B N′-1α-GFP, HA-H2B N′-tail-GFP, or HA-H2B αH-GFP, respectively]. To obtain full-length and truncated mutants of IPS-1, the full-length IPS-1 ORF (aa 1 to 540), aa 1 to 100, aa 91 to 180, aa 1 to 170, aa 1 to 100 plus aa 170 to 540, or aa 1 to 514 was either left alone or fused to the GFP ORF and then introduced into pCIneo-HA (HA-IPS-1 FL, HA-IPS-1 CARD-GFP, HA-IPS-1 PRD-GFP, HA-IPS-1-CARD-PRD, HA-IPS-1ΔPRD, or HA-IPS-1ΔTMD, respectively).

Yeast two-hybrid screening. Yeast two-hybrid screening was performed as described previously (25). Briefly, H2B cDNA was introduced in frame into the GAL4 DNA-binding domain of pGBKT7 as a bait plasmid (BD Clontech, Palo Alto, CA). A *Saccharomyces cerevisiae* strain, AH109, was transformed with a bait plasmid and the human bone marrow Matchmaker cDNA library (BD Clontech). After screening 1×10^6 clones on synthetic dropout selection agar plates (SD/-Leu/-Trp/-Ade/-His/5-bromo-4-chloro-3-indolyl-α-D-galactopyranoside; BD Clontech), positive clones were picked and the pACT2 library plasmids were recovered. The insert cDNA was sequenced and then characterized with the BLAST program.

Transient transfection and reporter gene assay. The cells (1×10^4) were transfected with 25 ng of pTK-RL (Promega) plus 25 ng of either reporter plasmid encoding an IFN-α4 or IFN-β promoter firefly luciferase (FFL) gene cassette (pGL3 IFN-α4 or pGL3 IFN-β) or pNF-κB-Luc (Stratagene). In some cases, the cells were cotransfected with expression plasmids for H2B, ZBP1, and RIG-I. Twenty-four hours after transfection, cells were stimulated with 0.1, 0.5, or 2.5 μg/ml of dsDNA [poly(dA·dT) or poly(dG·dC)] for 24 h or with 40 ng/ml of TNF-α for 8 h. The Dual-Glo luciferase assay system was used to measure both FFL activity and *Renilla* luciferase activity in the same sample. FFL activity of each sample was normalized against *Renilla* luciferase activity to obtain relative luciferase activity.

Pull-down assay. HEK293 cells were transiently transfected with H2B-FLAG and stimulated with 0.5 μg/ml of biotin-poly(dA·dT) or biotin-poly(dG·dC) for 4 or 16 h. Then, the cells were lysed in lysis buffer (25 mM Tris-HCl [pH 7.5], 1 mM EDTA, 0.1 mM EGTA, 5 mM $MgCl_2$, 100 mM NaCl, 10% glycerol, and 1% Nonidet P-40) containing both proteinase and phosphatase inhibitor cocktails (Sigma) on ice for 30 min. After centrifugation, the supernatants were recovered, mixed with streptavidin-agarose, and rotated at 4°C for 30 min. The complexes were washed with lysis buffer five times and suspended in SDS sample buffer, and then the supernatants were subjected to immunoblot analysis using anti-FLAG M2 Ab.

Viral genome binding assay. HEK293 cells were transiently transfected with hemagglutinin (HA)-GFP, HA-H2B FL-GFP, HA-H2B N′-tail-GFP, or HA-H2B αH-GFP. Twenty-four hours after the first transfection, the cells were transfected with pHPV18. Forty-eight hours after the second transfection, the cells were lysed in lysis buffer containing both proteinase and phosphatase inhibitor cocktails (Sigma) on ice for 30 min. After centrifugation, the supernatants were recovered and HA-fusion molecules were precipitated using anti-HA Ab. The complexes were washed with lysis buffer five times and then subjected to standard PCR targeting the subtype-specific E6 gene using the following primer set: HPV18 E6, 5′-CCT GCG GTG CCA GAA ACC GT-3′ and 5′-CGT TGG

AGT CGT TCC TGT CG-3′. The PCR products were separated on 2% agarose gels and visualized under UV light after ethidium bromide staining.

Immunoprecipitation and immunoblotting analysis. Immunoprecipitation and immunoblotting analyses were performed using anti-ZBP1 (clone RG7D12; kindly provided by Stefan Rothenburg [National Institutes of Health]), anti-H2B (BioVision, Mountain View, CA), anti-phospho-IRF-3 (Ser396) 4G4D, anti-IRF3 (Cell Signaling, Danvers, MA), anti-RIG-I (AnaSpec, Inc., San Jose, CA), anti-IPS-1 (MAVS) (Bethyl, Montgomery, TX), anti-importin 9, anti-glyceraldehyde-3-phosphate dehydrogenase (GAPDH) 6C5 (Abcam, Cambridge, United Kingdom), anti-Sp1, anti-STAT1, anti-extracellular signal-regulated kinase (ERK), anti-phospho-STAT1 (Santa Cruz Biotechnology, Santa Cruz, CA), anti-FLAG M2 (Sigma), or anti-HA Ab (Roche Diagnostics, Indianapolis, IN) as described previously (25).

FRET. For flow cytometric analysis of fluorescence resonance energy transfer (FRET), 293-F cells (Invitrogen) were transfected with cyan fluorescent protein (CFP) and/or yellow fluorescent protein (YFP) fusion proteins encoding histone H2B, IPS-1, or CIAO in 293 expression medium (Invitrogen) for 24 h, and measurements of YFP (excitation, 488 nm; emission, 530 nm), CFP (excitation, 407 nm; emission, 510 nm), FRET (excitation, 407 nm; emission, 535 nm) were performed using FACSAria (Becton Dickinson) and BD FACSDiVa software. FRET is shown as the YFP emission obtained by CFP excitation divided by the CFP emission by CFP excitation (11).

Transient replication of HPV. SCC-4 cells treated with control siRNA or H2B siRNA were transfected with the pHPV11 or -18 (VG012 and VG013; Human Science Research Resources Bank, Osaka, Japan) using Lipofectamine 2000 transfection reagent (Invitrogen). After incubation at 37°C for 24, 36, 60, or 72 h, the cells were washed with phosphate-buffered saline (PBS) and suspended in Hirt lysis buffer (0.6% SDS and 20 mM EDTA, pH 8.0). After 15 min, NaCl was added to a final concentration of 1 M, and then the mixture was placed at 4°C for 12 h. After centrifugation, the supernatants were treated with phenol-chloroform, and then DNA was precipitated with isopropanol. To distinguish replicated DNA from input DNA (pHPV11 or pHPV18), the samples were treated with DpnI endonuclease to degrade input DNA that had been propagated in *E. coli* DH5α. Resultant samples were suspended in Tris-EDTA, the concentrations were adjusted by measuring the optical density at 260 nm, and then 200 ng of DNA sample was subjected to standard PCR, targeting the subtype-specific E6 gene using the following primer sets: HPV11 E6, 5′-CTC CAC GTC TGC AAC ATC TA-3′ and 5′-TGA CAC AGG TAA CAA CGA AT-3′; HPV16 E6, 5′-CAC CAA AAG AGA ACT GCA ATG-3′ and 5′-TCA CGT CGC AGT AAC TGT TG-3′. The PCR products were separated on 2% agarose gels and visualized under UV light after ethidium bromide staining.

Virus multiplication study. Twenty-four hours after HEK293 or NIH 3T3 cells were infected with adenovirus (AdV) type 5 or MCMV strain MW97.01, respectively, total DNA was collected using a DNeasy tissue kit (Qiagen). One hundred nanograms of each sample was subjected to PCR using primers for the AdV hexon 5 gene, 5′-TGA AGC TGC TAC TGC TCT TGA A-3′ and 5′-GCA TTC AAC TGC CAT GCT TGG C-3′ (18 cycles), the human IFN-β gene promoter region (−110 to +20), 5′-CTA AAA TGT AAA TGA CAT AGG-3′ and 5′-AAA GGT TGC AGT TAG AAT GTC-3′ (18 cycles), the MCMV DNA polymerase gene, 5′-ACG CCG AGA AAG AGT ACG TGC TCA A-3′ and 5′-TCG GAC TGC ATC CTC TCG CAG TAG-3′ (22 cycles), or the mouse *Cd63* gene, 5′-GGT CTT GGG AAT TAT CTT CTC CTG CTG-3′ and 5′-CAC AGG CGG CAA AAT TCT TAA ACA TTC-3′ (26 cycles). After cell supernatants were recovered, the number of infectious viruses in 1 ml of each sample was determined by viral plaque assay or the 50% tissue culture infective dose ($TCID_{50}$) as described previously (10).

Statistical analysis. Student's *t* test was used for statistical analyses.

RESULTS

Identification of histone H2B as a mediator of dsDNA-induced IFN-β promoter activation. To identify molecules responsible for dsDNA-mediated type I IFN production in human cells, we screened a human bone marrow cDNA expression library using HEK293T cells stably expressing the *Luc* gene under the control of the IFN-β promoter. Among >960,000 independent clones examined, one of the positive clones encompassed the histone H2B1B ORF and exhibited a striking enhancement of dsDNA-induced IFN-β promoter activation (Fig. 1A). To confirm the role of histone H2B in dsDNA-induced innate immune responses, RNA interference was performed by using a small interfering RNA (siRNA). H2B siRNA treatment significantly suppressed the level of H2B protein expression (see Fig. S1 in the supplemental material). H2B siRNA also suppressed the levels of IFN-β production and IFN regulatory factor 3 (IRF3) phosphorylation induced by dsDNA in HEK293 cells (Fig. 1B and C, respectively), and knockdown of histone H2B inhibited dsDNA-induced activation of various gene promoters regulating IFN-related gene expression (see Fig. S2 in the supplemental material). dsDNA stimulates IRF kinases, such as TBK1 and IKKi (6). Overexpression of TBK1 and IKKi elicited comparable levels of IFN-β production in both control and H2B knockdown HEK293 cells, suggesting that H2B functions upstream of these kinases (Fig. 1D). To confirm the intracellular interaction of histone H2B and dsDNA, we performed pull-down and immunoprecipitation analyses. As a result, histone H2B was coprecipitated with biotinylated poly(dA·dT) or poly(dG·dC) that had been transfected into cells (Fig. 1E). To further identify the dsDNA interaction domain of histone H2B, we performed immunoprecipitation analysis using H2B mutants. It was found that the COOH-terminal α-helical region (αH domain) of histone H2B is sufficient for the interaction with HPV DNA (Fig. 1F). Furthermore, complementation of full-length histone H2B in knockdown cells restored the levels of IFN-β promoter activation induced by dsDNA but not that of the NH_2-terminal tail region (N′-tail) or the αH domain alone (Fig. 1G). These results suggest that histone H2B binds to dsDNA through the αH domain, but both the N′-tail and αH domain are required for dsDNA-mediated signaling. When different siRNAs, each targeting histone H1, H2A, H2B, H3, or H4 were tested, only H2B siRNA attenuated IFN-β promoter activation induced by dsDNA (Fig. 1H). Such an effect of H2B siRNA was not observed following dsRNA or TNF-α stimulation (Fig. 1H). These results suggest that histone H2B is involved in the signal activation triggered by dsDNA.

Histone H2B is involved in the signal activation triggered by dsDNA but not that by dsRNA nor TLR ligands. ZBP1 or RIG-I is known as a cytosolic DNA sensor in a mouse connective tissue cell line, L929, and a human hepatoma cell line, Huh7, respectively. dsDNA-induced IFN-β promoter activation was significantly suppressed in the cells treated with histone H2B siRNA, but not with siRNA targeting ZBP1 or RIG-I (Fig. 2A), although each siRNA specifically downregulated the level of target protein expression in HEK293 cells (Fig. 2B). Knockdown of histone H2B resulted in a suppression of IFN-β production in response to dsDNA, but not to 5′-triphosphate RNA stimulation in HUVEC (Fig. 2C). Alt hough histone H2B is an essential component of the chromosome, H2B knockdown cells used in our present study could normally proliferate and respond to TNF-α or Toll-like receptor (TLR) ligands comparably to those treated with con trol siRNA (Fig. 2D and E), suggesting that chromosomal histone H2B that is essential for cell survival or TNF receptor (TNFR)- or TLR-mediated signaling pathways were not impa ired by the use of these siRNAs. These results *in toto* suggest that histone H2B is involved in the signal activation triggered by dsDNA, but not that by dsRNA or TLR ligands.

Extrachromosomal histone H2B associates with IPS-1 in the cytoplasm. Immunofluorescence analysis revealed that al-

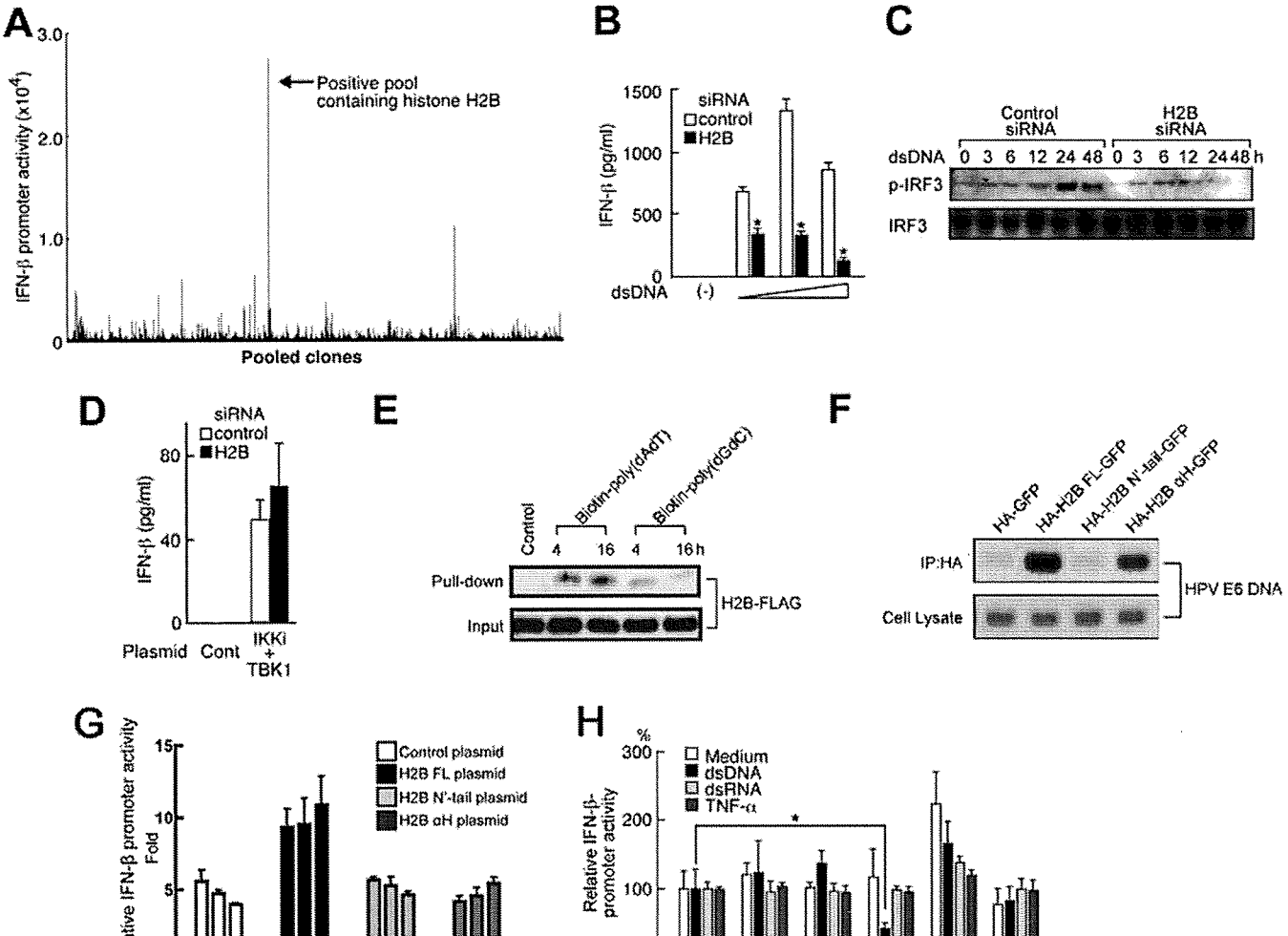

FIG. 1. Histone H2B mediates dsDNA-induced cellular activation. (A) A human bone marrow expression cDNA library was screened based on the ability to mediate dsDNA-induced IFN-β promoter activation. (B to D) HEK293 cells were transfected with control siRNA or siRNA targeting H2B. (B) The cells were treated with 0, 0.1, 0.5, or 2.5 μg/ml of dsDNA [poly(dA·dT)], and the supernatants were subjected to an enzyme-linked immunosorbent assay (ELISA) for IFN-β (PBL). (C) The cells were treated with 0.5 μg/ml of dsDNA [poly(dA·dT)] for 0, 3, 6, 12, 24, and 48 h, and the levels of phosphorylated IRF3 (p-IRF3) in the nucleus and IRF3 (normalization control) in the whole-cell lysates were examined by immunoblotting analysis. (D) The cells were further transfected with expression plasmids for TBK1 and IKKi, and the supernatants were subjected to ELISA for IFN-β (PBL). (E) HEK293 cells were transfected with histone H2B-FLAG and treated with biotin-poly(dA·dT) or biotin-poly(dG·dC). The cell lysates were collected, and a pull-down assay was performed with streptavidin-agarose. The complex was analyzed by immunoblotting using anti-FLAG Ab. (F) HEK293 cells were transfected with HA-GFP, HA-H2B-GFP, HA-H2B N′-tail-GFP, or HA-H2B αH-GFP. Twenty-four hours after the first transfection, the cells were further transfected with the HPV18 genome. Forty-eight hours after the second transfection, the cell lysates were collected and immunoprecipitation was performed with anti-HA Ab. The standard PCR targeting the HPV18 E6 gene was conducted with each cell lysate and immunoprecipitated complex. (G) HEK293 cells were transfected with H2B siRNA and then further transfected with pGL3 IFN-β and pTK-RL plus control, H2B FL, the H2B N′-tail, or the H2B αH plasmid. After treatment with 0, 0.1, 0.5, or 2.5 μg/ml of dsDNA [poly(dA·dT)] for 24 h, a luciferase assay was performed. (H) HEK293 cells were transfected with control siRNA or siRNA targeting either H2B, H1, H2A, H3, or H4. The cells were further transfected with pGL3 IFN-β and pTK-RL and treated with or without 0.5 μg/ml of dsDNA [poly(dA·dT)], dsRNA [poly(I:C)], or TNF-α (50 ng/ml) for 24 h, and then a luciferase assay was performed. The luciferase activity is depicted as the IFN-β promoter activity relative to samples obtained from the cells treated with control siRNA in each stimulation (relative IFN-β promoter activity). All data except for those in panel represent means ± standard deviations (SD) of six to eight samples. *, $P < 0.05$.

though most histone H2B colocalized with Hoechst staining (chromosomes), there was some H2B staining in the extrachromosomal area (Fig. 3A). The levels of such extrachromosomal H2B were diminished when cells were treated with H2B siRNA, while chromosomal H2B in the same cell was present at a level similar to that in the control cells. Since it is known that histones are also released from the nucleus (14), the levels of histone H2B in each cellular fraction were evaluated by immunoblotting analysis. In accordance with the results of immunofluorescence analysis, H2B siRNA significantly de-

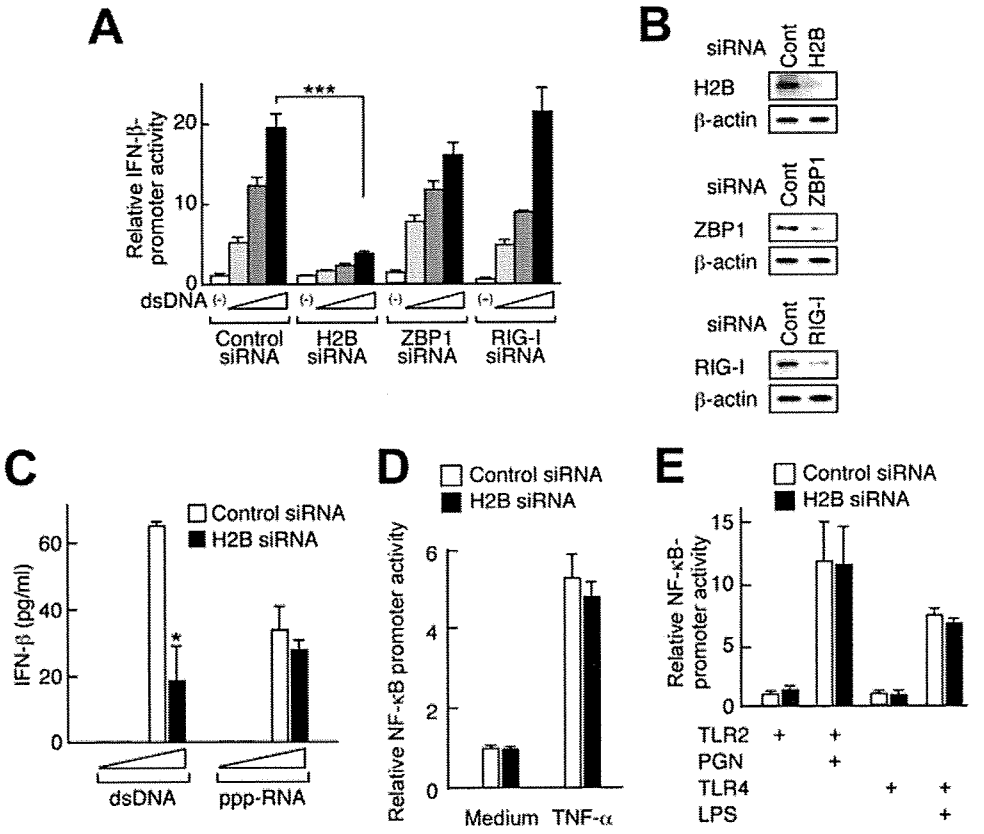

FIG. 2. Histone H2B is involved in the signal activation triggered by dsDNA, but not that of dsRNA or TLR ligands. HEK293 (A, B, D, and E) or HUVEC (C) cells were transfected with control siRNA or siRNA targeting either H2B, ZBP1, or RIG-I. (A and B) The cells were further transfected with expression plasmids for histone H2B, ZBP1, and RIG-I, in the presence of pGL3 IFN-β plus pTK-RL. (A) Twenty-four hours after transfection, cells were treated with 0, 0.1, 0.5, or 2.5 μg/ml of dsDNA [poly(dA·dT)] for 24 h, and then a luciferase assay was performed. (B) Twenty-four hours after transfection, levels of protein expression were examined by immunoblotting analysis using anti-RIG-I, anti-ZBP1, anti-H2B, or anti-β-actin Ab. (C) The cells were treated with 0.1 or 1.0 μg/ml of dsDNA [poly(dA·dT)] or 5′-triphosphate RNA (ppp-RNA) for 24 h, and the supernatants were subjected to an ELISA for IFN-β. (D) The cells were further transfected with pNF-κB-Luc plus pTK-RL and treated with or without TNF-α (50 ng/ml) for 8 h, and then a luciferase assay was performed. (E) The cells were further transfected with pNF-κB-Luc plus pTK-RL in the presence of either expression plasmid for TLR2 or TLR4 plus MD2 and treated with or without peptidoglycan (PGN; 1 μg/ml) or lipopolysaccharide (LPS; 100 ng/ml) for 24 h, and then a luciferase assay was performed. *, $P < 0.05$; ***, $P < 0.001$.

creased extrachromosomal H2B, but not choromosomal H2B (Fig. 3B). Only when the cells were stimulated with dsDNA for 12 h, but not when they were stimulated with dsRNA, was a punctate signal of H2B fluorescence detected in the cytoplasm (Fig. 3C), suggesting that dsDNA induces aggregation of histone H2B in the cytoplasm. Of interest, the colocalization of H2B with IPS-1 was observed following dsDNA stimulation (Fig. 3C, magenta arrows). To further examine the molecular interaction between histone H2B and IPS-1, immunoprecipitation analysis was performed. The cytoplasmic extracts and postchromosomal nuclear extracts were segregated from HEK293 cells stimulated with or without dsDNA. The purity of each extract was confirmed by immunoblotting analysis with anti-GAPDH (a cytoplasmic enzyme) or anti-Sp1 (a nuclear transcription factor) Ab as shown in Fig. 3D. IPS-1 was predominantly present in the cytoplasmic extracts, while histone H2B was in both extracts. When IPS-1 was immunoprecipitated from the cytoplasmic extracts, coprecipitation of histone H2B was not detected before stimulation but was detected 12 h after dsDNA stimulation. In contrast, when H2B was immunoprecipitated from the nuclear extracts, no detectable IPS-1 coprecipitated even after dsDNA stimulation. Taken together, these results suggest that the interaction between histone H2B and IPS-1 takes place in the cytoplasm following dsDNA stimulation.

Identification of CIAO as a species-specific molecule that links histone H2B and IPS-1. To identify the molecules directly associating with histone H2B, yeast two-hybrid screening was performed. As a result, 3 out of 10 positive clones were identified as KIAA1192, whose function has not yet been characterized but this nucleotide sequence is identical to the COOH-terminal end of importin 9, as a possible alternative splicing transcript of importin 9 (see Table S1 in the supplemental material). We renamed it to CIAO, based on its novel role, described below. Immunoprecipitation analysis clearly revealed that CIAO binds to histone H2B as well as IPS-1 but not to RIG-I (Fig. 4A). Full-length importin 9 interacted with histone H2B but not with IPS-1 (data not shown), suggesting that CIAO, a possible alternative splicing variant of importin 9, gains a peculiar function as an interacting partner of IPS-1. The spatial disposition of H2B, CIAO, and IPS-1 in the cell was further examined by FRET analysis. As shown in Fig. 4B,

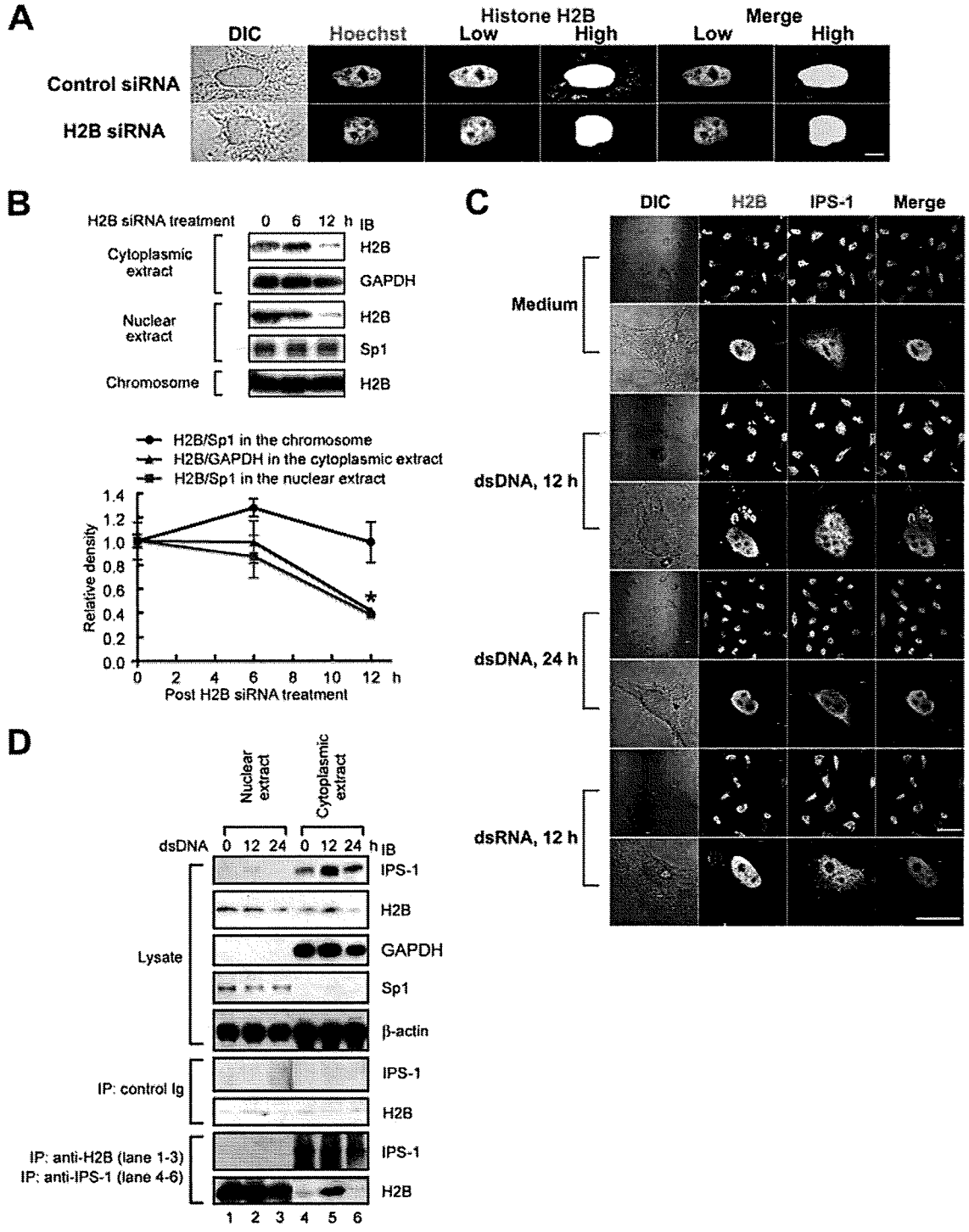

FIG. 3. Extrachromosomal histone H2B interacts with IPS-1. (A) HeLa cells were transfected with control or H2B siRNA. Twelve hours after transfection, the cells were fixed, stained with Hoechst 33258 and anti-H2B Ab followed by Alexa 488-conjugated anti-mouse IgG Ab, and then examined under a confocal microscope. The pictures taken under low and high lighting conditions are shown as low and high, respectively. Bar, 20 μm. (B) The cells were collected 0, 6, or 12 h after H2B siRNA treatment, and the cell lysates were fractionated into the cytoplasmic extract, the nuclear extract, and the chromosome fraction. Each fraction was analyzed by immunoblotting using anti-H2B, anti-GAPDH, or anti-Sp1 Ab. The density of each H2B band was normalized to the density of the corresponding GAPDH band (the cytoplasmic extract) or Sp1 band (the nuclear extract and the chromosome fraction) and is shown on the graph ($n = 3$). (C) After stimulation with or without dsDNA or dsRNA for 12 or 24 h, HeLa cells were fixed and stained with anti-H2B Ab and anti-IPS-1 Ab followed by Alexa 488-conjugated anti-mouse IgG Ab and Alexa 555-conjugated anti-rabbit IgG Ab. The cells were then examined under a confocal microscope. Bar, 100 μm in low-magnification pictures (upper panels) and 50 μm in high-magnification pictures (lower panels). (D) HEK293 cells were collected 0, 12, or 24 h after dsDNA stimulation, and the cell lysates were fractionated into the cytoplasmic extract and nuclear extract. Each fraction was immunoprecipitated with control IgG, anti-H2B, or anti-IPS-1 Ab. The immune complexes were analyzed by immunobloting using either anti-H2B or anti-IPS-1 Ab. *, $P < 0.05$.

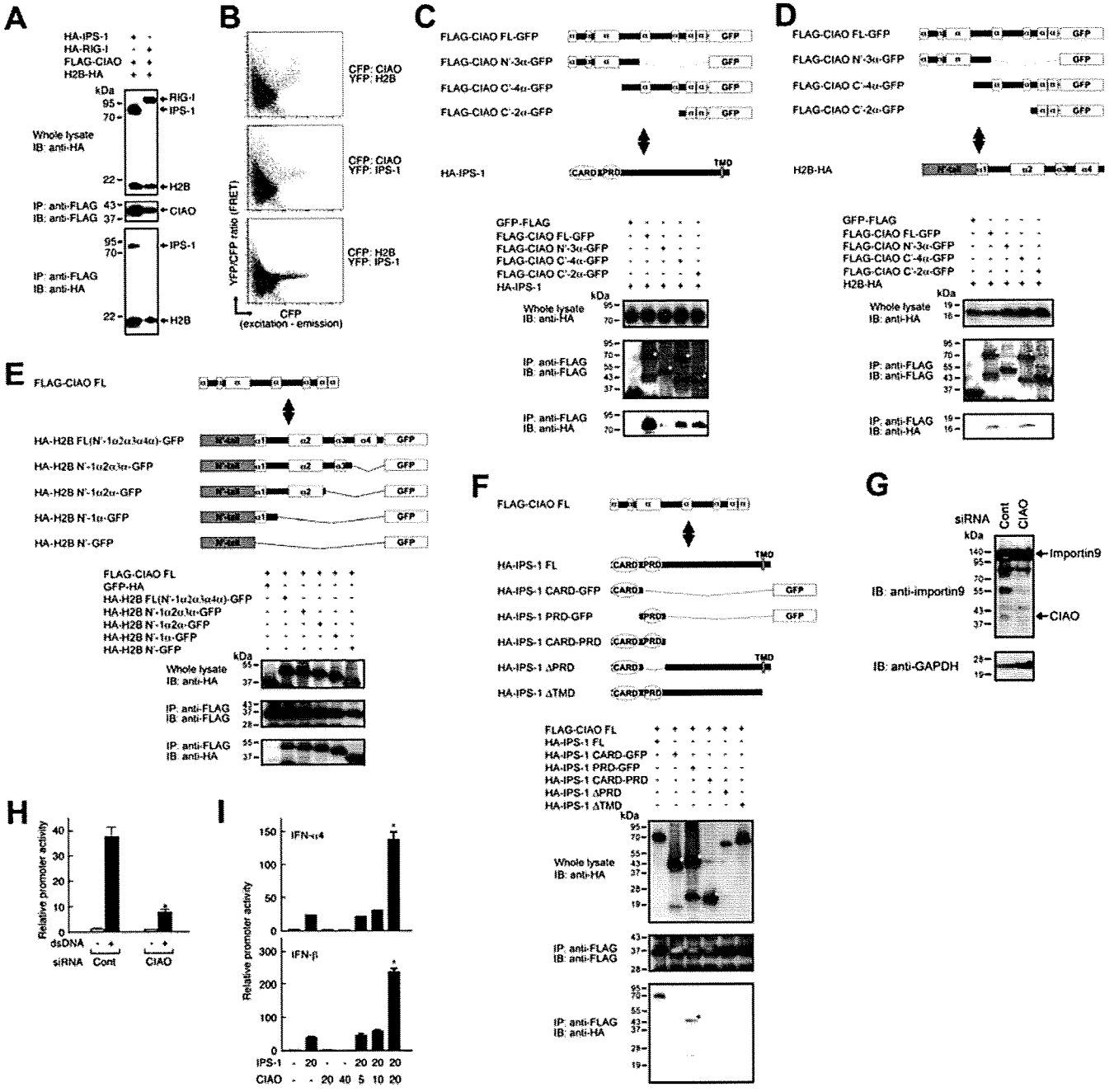

FIG. 4. CIAO associates with histone H2B and IPS-1 to constitute a signaling complex, thereby transmitting a signal leading to type I IFN production. (A and C to F) Cell lysates from HEK293 cells transfected with the indicated expression plasmid were immunoprecipitated with anti-FLAG Ab. The immune complexes were analyzed by immunoblotting using either anti-HA or anti-FLAG Ab. (B) 293-F cells transfected with CFP and YFP fusion proteins encoding histone H2B, IPS-1, or CIAO. FRET results are shown as the YFP emission obtained by CFP excitation divided by the CFP emission by CFP excitation. (C to F) Schematic diagrams of CIAO, IPS-1, H2B, and their truncated mutants. α, a putative α-helical region of CIAO and H2B; *, a predicted gene product of the target molecule. (G) HeLa cells were transfected with control siRNA or CIAO siRNA. Immunoblotting analysis was conducted using anti-importin 9 (COOH-terminal end) monoclonal Ab. (H and I) HeLa cells were transfected with or without the indicated reporter plasmid plus the indicated amounts (in ng) of expression plasmid(s). A luciferase assay was performed as described for Fig. 1. Data represent means ± SD of the relative luciferase activity of six to eight samples. *, $P < 0.05$.

the higher levels of the specific FRET signal were detected in cells expressing CFP-CIAO and YFP-H2B as well as CFP-CIAO and YFP-IPS-1, compared to those expressing CFP-H2B and YFP-IPS-1, suggesting that CIAO and H2B or CIAO and IPS-1 juxtapose in a close spatiality and that CIAO disposes between H2B and IPS-1 in a molecular complex, thereby acting as an adaptor linking histone H2B to IPS-1. We further characterized the domains of CIAO, histone H2B, and IPS-1 that are responsible for the molecular interaction. Immunoprecipitation analysis demonstrated that the COOH-terminal

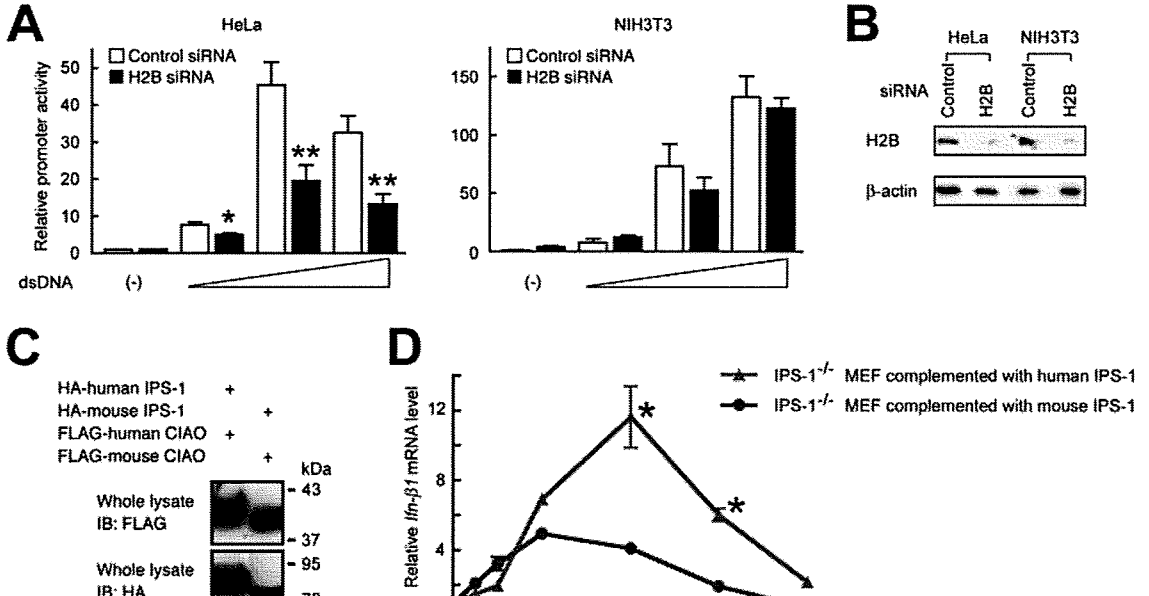

FIG. 5. Species-specific involvement of histone H2B and IPS-1 in dsDNA-mediated signaling. (A and B) HeLa or NIH 3T3 cells were transfected with either control or H2B siRNA. (A) The cells were further transfected with pGL3 IFN-β and pTK-RL and treated with 0, 0.1, 0.5, or 2.5 μg/ml of dsDNA [poly(dA·dT)] for 24 h, and then a luciferase assay was performed. (B) The levels of H2B protein expression were examined by immunoblotting analysis. (C) The immunoprecipitation analysis was performed after HEK293 cells were transfected with the expression plasmids for human or mouse IPS-1 and CIAO. (D) IPS-$1^{-/-}$ MEF stably complemented with mouse or human IPS-1 were stimulated with 0.5 μg/ml of dsDNA [poly(dA·dT)] for 3, 6, 12, 24, 36, and 48 h. The cells were subjected to real-time PCR analysis for *Ifnb1* mRNA and 18S rRNA. The levels of *Ifnb1* mRNA were normalized with the corresponding levels of 18S rRNA and are shown on the graph ($n = 4$). *, $P < 0.05$; **, $P < 0.01$.

region of CIAO (aa 194 to 249) is sufficient to interact with IPS-1, while the central region of CIAO (aa 91 to 193) is required for interaction with H2B (Fig. 4C and D). The N′-tail of H2B (aa 1 to 37) is sufficient, while the proline-rich domain (PRD) of IPS-1 (aa 94 to 170) is required for the interaction with CIAO (Fig. 4E and F). CIAO was endogenously expressed in HeLa and HEK293 cells (Fig. 4G and data not shown), and the treatment of siRNA targeting the CIAO ORF significantly suppressed the expression level of CIAO but not importin 9 protein (Fig. 4G). Knockdown of CIAO resulted in a marked reduction in dsDNA-induced activation of the IFN-β promoter (Fig. 4H), while overexpression of CIAO enhanced IPS-1-induced activation of type I IFN promoters (Fig. 4I). Taken together, these results indicate that CIAO links histone H2B to IPS-1, thereby enabling H2B-mediated type I IFN production in human cells.

Species-specific involvement of histone H2B and IPS-1 in dsDNA-mediated signaling. Previous reports have demonstrated that there are mechanistic differences in dsDNA signaling among species, e.g., human IPS-1 but not mouse IPS-1 is involved in dsDNA-mediated cellular signaling (2, 6, 15, 22). To examine a molecular mechanism underlying the species-specific signaling pathway induced by dsDNA, we compared the effects of H2B knockdown in human and mouse cells. Our results showed that knockdown of H2B resulted in a suppression of dsDNA-mediated IFN-β promoter activation in HeLa cells but not in NIH 3T3 cells (Fig. 5A and B), suggesting that there is a difference in the action of histone H2B between these species. Of interest, however, although an interaction was observed between human CIAO and IPS-1, an interaction between mouse CIAO and IPS-1 was not observed (Fig. 5C). While high similarities of amino acid sequences were seen among human and mouse H2B subtypes (human H2B1A, -1B, -1C, -1D, -1H, -1J, -1K, -1L, -1M, -1N, -1O, -2E, -2F, -3B, and -FS and mouse H2B1A, -1B, -1C, -1F, -1H, -1K, -1M, -1P, and -3A) (>70.1%) and between human and mouse CIAO (99.2%), a lower level of identity was seen between human and mouse IPS-1 amino acid sequences (30.3%). Thus, it was suggested that human IPS-1, but not mouse IPS-1, has the potential to interact with histone H2B and transmit signaling. To further examine a human IPS-1-specific mechanism in dsDNA-mediated signaling, we complemented $IPS^{-/-}$ mouse embryonic fibroblasts (MEF) with mouse IPS-1 (mouse IPS-1 MEF) or human IPS-1 (human IPS-1 MEF) and tested their responses to dsDNA. While *Ifnb1* mRNA expression was induced within 3 h, its level peaked at 12 h after dsDNA stimulation and thereafter declined in mouse IPS-1 MEF (Fig. 5D). In contrast, the level of *Ifnb1* mRNA expression peaked at 24 h after dsDNA stimulation in human IPS-1 MEF, and the overall level was significantly higher in human IPS-1 MEF than in mouse IPS-1 MEF (Fig. 5D). Thus, these results, taken together, suggest that human IPS-1 mediates the later-phase induction of IFN-β compared with that mediated by the dsDNA signaling endogenously present in MEF (Fig. 5D).

Extrachromosomal histone H2B is involved in suppression of DNA virus multiplication. We further evaluated the biolog-

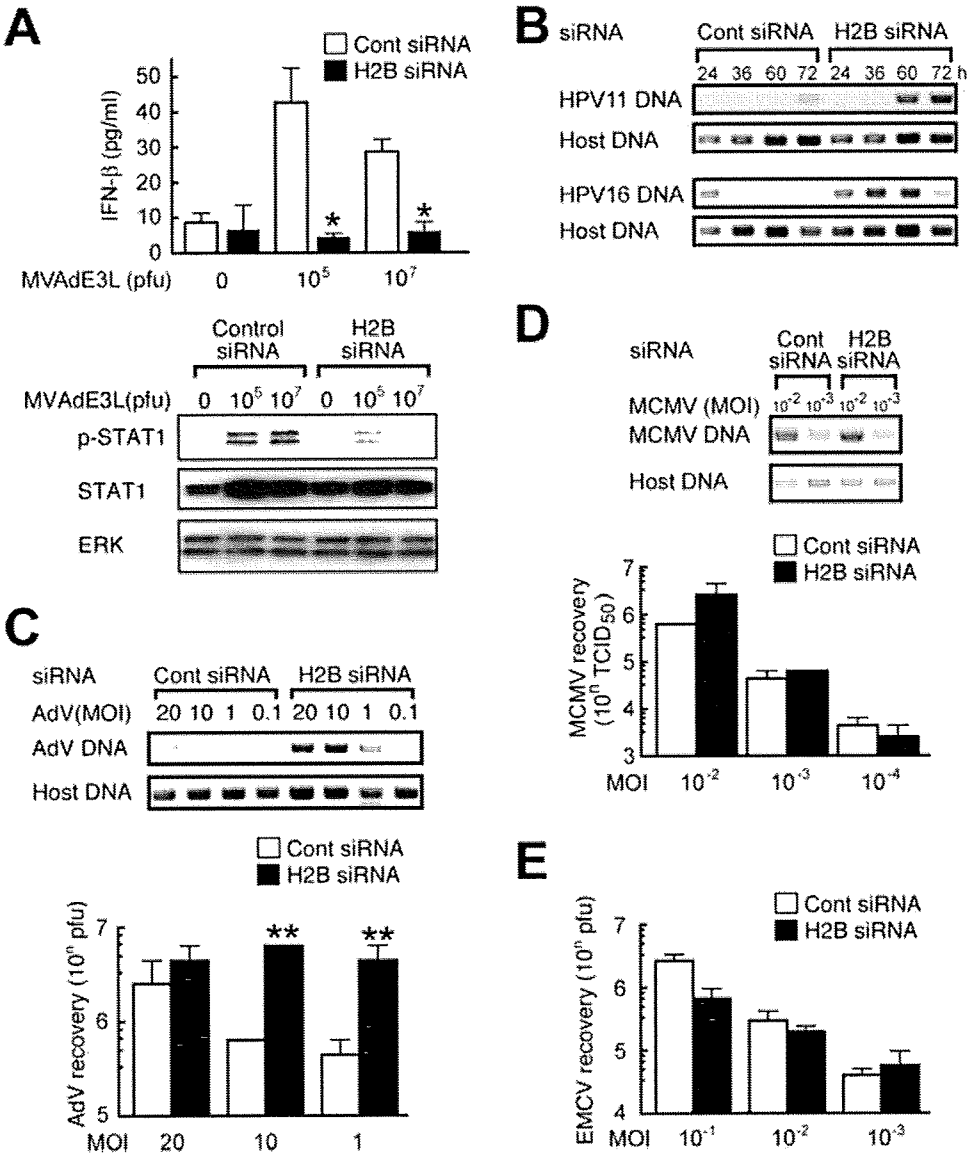

FIG. 6. Histone H2B is a crucial element for suppression of DNA virus replication. (A to E) HEK293 (A and C), SCC-4 (B), NIH 3T3 (D), or HeLa cells (E) were pretreated with control siRNA or H2B siRNA. (A) The cells were infected with MVAdE3L (1×10^5 or 1×10^7 PFU). Twenty-four hours after infection, cell lysates were subjected to immunoblotting for total STAT1, phosphorylated STAT1 (p-STAT1), or ERK. (B) The cells were transfected with the HPV11 or -16 genome, and the episomal DNA fractions were recovered 24, 36, 60, or 72 h after transfection. Viral multiplication was determined by PCR. (C and D) The cells were infected with AdV type 5 or MCMV strain MW97.01. Twenty-four hours after infection, viral multiplication was determined by PCR amplification of the viral genomic DNA and by a plaque assay (AdV) or by measuring the $TCID_{50}$ (MCMV). (E) The cells were infected with EMCV. Twenty-four hours after infection, viral multiplication was determined by a plaque assay. *, $P < 0.05$; **, $P < 0.01$.

ical role of histone H2B on cell-autonomous antiviral responses. Knockdown of histone H2B suppressed vaccinia virus-induced IFN-β production as well as STAT1 phosphorylation (Fig. 6A). Multiplication of human papilloma viruses (HPV 11 and HPV 16) and AdV type 5 was significantly enhanced in the H2B knockdown cells (Fig. 6B and C, respectively) but not in RIG-I or ZBP-1-knockdown cells (see Fig. S3 in the supplemental material). H2B knockdown, however, had virtually no effect on the multiplication of MCMV in mouse cells and RNA virus, EMCV, in human cells (Fig. 6D and E). These findings suggest that extrachromosomal histone H2B is involved in a sensing mechanism of DNA virus infection and mediates cell-autonomous antiviral innate immune responses in human cells.

DISCUSSION

Our results provide direct evidence indicating that extrachromosomal histone H2B plays an important role in the signaling pathway triggered by dsDNA. Biologically, dsDNA is released following unusual or "dangerous" situations in cells, e.g., infection, apoptosis, and tissue damage (6, 18, 23). Therefore, the signaling pathway mediated by the signalsome con-

sisting of extrachromosomal histone H2B and IPS-1 may have evolved not just in response to pathogen recognition but also perhaps for auto-recognition of unusual self DNA.

Although histone H2B is usually assembled in the nucleosome as a core histone, histone exchange and deposition often take place in living cells, with ~3% of total H2B having a $t_{1/2}$ of ~6 min, ~40% with a $t_{1/2}$ of ~130 min, and >50% with a $t_{1/2}$ of ~8.5 h. Indeed, nucleosome assembly protein 1 mediates chromatin fluidity by exchanging H2A/H2B and assisting nucleosome sliding (13). Nuclear import of the cytoplasmic core histones occurs along multiple redundant pathways mediated by importin family members. Importin 9 mediates one of the most productive pathways in H2B import through the nuclear core complex (8, 17). Interestingly, karyopherin 114p, a yeast homologue of mammalian importin 9, bind to the H2A-H2B complex in the cytoplasm (16). Such evidence strongly supports our present observation that the extrachromosomal H2B that is released from the chromosome plays an important role in the signal transmission induced by dsDNA.

Lines of evidence in recent decades indicate how histones are assembled with the genomic DNA to compose the chromosomes. Most studies have focused on the assumption that histones target only the genomic DNA under physiological conditions. Recent studies, however, have demonstrated that subtypes of histones play distinct roles in extrachromosomal settings. H2A.X is phosphorylated and recruited where DNA double-strand breaks take place (19), and H3.3 accumulates in the condensed chromatin where gene transcription is activated (9). More striking evidence is that H1.2 transmigrates from the nucleus to mitochondria to transmit apoptotic signals arising from DNA damage, and this crucially regulates the Bak-dependent release of cytochrome *c* from mitochondria (14). Thus, further characterization of extrachromosomal histone H2B as a component of the signaling complex may help in understanding the biological roles of the extrachromosomal histones and the mechanism of cell-autonomous protection against invading pathogens after dsDNA sensing.

CIAO encodes a 750-bp ORF identical to the COOH-terminal end of the importin 9 ORF (aa 793 to 1041) with no apparent domains or regions responsible for signal transduction. Although we have identified that the COOH-terminal region of CIAO is sufficient for the interaction with the IPS-1 PRD and the central region of CIAO is required for the interaction with the NH_2-terminal tail region of H2B, the dynamics of such signaling complex formation under physiological conditions or during viral infection remain to be elucidated. To examine such dynamics, we are now generating Ab and agents to discriminate endogenous CIAO from importin 9 or the extrachromosomal histone H2B from the chromosomal histone by targeting specific residues of each molecule that have been modified before or after the complex formation.

It has been demonstrated that RIG-I plays a significant role in dsDNA-induced antiviral responses through IPS-1 in the human hepatoma cell line, Huh7 (2). However, we observed that histone H2B but not RIG-I or ZBP1 is involved in dsDNA-mediated signaling in HEK293 cells, suggesting that there are some cell-type-specific as well as redundant mechanisms in the signaling pathway activated by dsDNA. In fact, although ZBP1, also known as DAI, is involved in dsDNA-mediated signaling in mouse L929 cells, its *in vivo* role is redundant (7, 24).

The present data indicate that extrachromosomal histone H2B recognizes and interacts with not only "transfected" dsDNA but also viral DNA exposed to the cytoplasm. This mechanism is crucial for cell-autonomous innate responses to infection with vaccinia virus, AdV, and HPV, but not with EMCV. Our ongoing analysis shows that replication of HIV is also enhanced in H2B knockdown Magic5 cells (data not shown), suggesting that proviral dsDNA rather than genomic RNA of HIV is sensed by extrachromosomal histone H2B. Thus, histone H2B seems to discriminate between foreign DNA and RNA upon viral infection to evoke IPS-1-mediated signaling through the association with a novel adaptor protein, CIAO, and it is suggested that human IPS-1 has evolutionarily gained the potential to transmit dsDNA- and histone H2B-mediated signaling to combat against human viruses that produce DNA intermediates within the cell.

In conclusion, our present work demonstrates that extrachromosomal histone H2B physically interacts with IPS-1 through CIAO to form a distinct signaling complex that transmits dsDNA-induced type I IFN production in human cells. Such a molecular platform may act as a sensor of the dsDNA aberrantly present within the cell, alerting cells to urgent hazards, such as pathogens (infection), apoptosis (hormonal stimuli, chemical agents, or irradiation), and necrosis (injury). Thus, this mechanism may also play some roles in autoimmunity, transplantation rejection, gene-mediated vaccines, and other therapeutic applications.

ACKNOWLEDGMENTS

We declare no conflicts of interest.

This work was supported in part by the Strategic Research Project of Yokohama City University (K18022 to F.T.), Advancement of Medical Sciences from Yokohama Medical Foundation (to F.T.), the National Institute of Biomedical Innovation (to K.O.), Mitsubishi Pharma Research Foundation (to K.S.), and a Grant-in-Aid for Scientific Researches (B and C) and Innovative Areas (18590432, 20590477, and 20200074 to F.T., 18659126 to K.O., and 15390296 to K.S.) from the Ministry of Education, Culture, Sports, Science, and Technology of Japan and from the Japan Science and Technology Corporation.

REFERENCES

1. **Burckstummer, T., C. Baumann, S. Bluml, E. Dixit, G. Durnberger, H. Jahn, M. Planyavsky, M. Bilban, J. Colinge, K. L. Bennett, and G. Superti-Furga.** 2009. An orthogonal proteomic-genomic screen identifies AIM2 as a cytoplasmic DNA sensor for the inflammasome. Nat. Immunol. **10**:266–272.
2. **Cheng, G., J. Zhong, J. Chung, and F. V. Chisari.** 2007. Double-stranded DNA and double-stranded RNA induce a common antiviral signaling pathway in human cells. Proc. Natl. Acad. Sci. U. S. A. **104**:9035–9040.
3. **Fernandes-Alnemri, T., J. W. Yu, P. Datta, J. Wu, and E. S. Alnemri.** 2009. AIM2 activates the inflammasome and cell death in response to cytoplasmic DNA. Nature **458**:509–513.
4. **Hornung, V., A. Ablasser, M. Charrel-Dennis, F. Bauernfeind, G. Horvath, D. R. Caffrey, E. Latz, and K. A. Fitzgerald.** 2009. AIM2 recognizes cytosolic dsDNA and forms a caspase-1-activating inflammasome with ASC. Nature **458**:514–518.
5. **Isaacs, A., R. A. Cox, and Z. Rotem.** 1963. Foreign nucleic acids as the stimulus to make interferon. Lancet **ii**:113–116.
6. **Ishii, K. J., C. Coban, H. Kato, K. Takahashi, Y. Torii, F. Takeshita, H. Ludwig, G. Sutter, K. Suzuki, H. Hemmi, S. Sato, M. Yamamoto, S. Uematsu, T. Kawai, O. Takeuchi, and S. Akira.** 2006. A Toll-like receptor-independent antiviral response induced by double-stranded B-form DNA. Nat. Immunol. **7**:40–48.
7. **Ishii, K. J., T. Kawagoe, S. Koyama, K. Matsui, H. Kumar, T. Kawai, S. Uematsu, O. Takeuchi, F. Takeshita, C. Coban, and S. Akira.** 2008. TANK-binding kinase-1 delineates innate and adaptive immune responses to DNA vaccines. Nature **451**:725–729.

8. **Jakel, S., J. M. Mingot, P. Schwarzmaier, E. Hartmann, and D. Gorlich.** 2002. Importins fulfil a dual function as nuclear import receptors and cytoplasmic chaperones for exposed basic domains. EMBO J. **21**:377–386.
9. **Janicki, S. M., T. Tsukamoto, S. E. Salghetti, W. P. Tansey, R. Sachidanandam, K. V. Prasanth, T. Ried, Y. Shav-Tal, E. Bertrand, R. H. Singer, and D. L. Spector.** 2004. From silencing to gene expression: real-time analysis in single cells. Cell **116**:683–698.
10. **Jounai, N., F. Takeshita, K. Kobiyama, A. Sawano, A. Miyawaki, K. Q. Xin, K. J. Ishii, T. Kawai, S. Akira, K. Suzuki, and K. Okuda.** 2007. The Atg5 Atg12 conjugate associates with innate antiviral immune responses. Proc. Natl. Acad. Sci. U. S. A. **104**:14050–14055.
11. **Kawai, T., S. Sato, K. J. Ishii, C. Coban, H. Hemmi, M. Yamamoto, K. Terai, M. Matsuda, J. Inoue, S. Uematsu, O. Takeuchi, and S. Akira.** 2004. Interferon-alpha induction through Toll-like receptors involves a direct interaction of IRF7 with MyD88 and TRAF6. Nat. Immunol. **5**:1061–1068.
12. **Kawane, K., M. Ohtani, K. Miwa, T. Kizawa, Y. Kanbara, Y. Yoshioka, H. Yoshikawa, and S. Nagata.** 2006. Chronic polyarthritis caused by mammalian DNA that escapes from degradation in macrophages. Nature **443**:998–1002.
13. **Kimura, H.** 2005. Histone dynamics in living cells revealed by photobleaching. DNA Repair (Amst.) **4**:939–950.
14. **Konishi, A., S. Shimizu, J. Hirota, T. Takao, Y. Fan, Y. Matsuoka, L. Zhang, Y. Yoneda, Y. Fujii, A. I. Skoultchi, and Y. Tsujimoto.** 2003. Involvement of histone H1.2 in apoptosis induced by DNA double-strand breaks. Cell **114**: 673–688.
15. **Kumar, H., T. Kawai, H. Kato, S. Sato, K. Takahashi, C. Coban, M. Yamamoto, S. Uematsu, K. J. Ishii, O. Takeuchi, and S. Akira.** 2006. Essential role of IPS-1 in innate immune responses against RNA viruses. J. Exp. Med. **203**:1795–1803.
16. **Mosammaparast, N., K. R. Jackson, Y. Guo, C. J. Brame, J. Shabanowitz, D. F. Hunt, and L. F. Pemberton.** 2001. Nuclear import of histone H2A and H2B is mediated by a network of karyopherins. J. Cell Biol. **153**:251–262.
17. **Muhlhausser, P., E. C. Muller, A. Otto, and U. Kutay.** 2001. Multiple pathways contribute to nuclear import of core histones. EMBO Rep. **2**:690–696.
18. **Napirei, M., H. Karsunky, B. Zevnik, H. Stephan, H. G. Mannherz, and T. Moroy.** 2000. Features of systemic lupus erythematosus in Dnase 1-deficient mice. Nat. Genet. **25**:177–181.
19. **Redon, C., D. Pilch, E. Rogakou, O. Sedelnikova, K. Newrock, and W. Bonner.** 2002. Histone H2A variants H2AX and H2AZ. Curr. Opin. Genet. Dev. **12**:162–169.
20. **Roberts, T. L., A. Idris, J. A. Dunn, G. M. Kelly, C. M. Burnton, S. Hodgson, L. L. Hardy, V. Garceau, M. J. Sweet, I. L. Ross, D. A. Hum, and K. J. Stacey.** 2009. HIN-200 proteins regulate caspase activation in response to foreign cytoplasmic DNA. Science **323**:1057–1060.
21. **Stetson, D. B., and R. Medzhitov.** 2006. Recognition of cytosolic DNA activates an IRF3-dependent innate immune response. Immunity **24**:93–103.
22. **Sun, Q., L. Sun, H. H. Liu, X. Chen, R. B. Seth, J. Forman, and Z. J. Chen.** 2006. The specific and essential role of MAVS in antiviral innate immune responses. Immunity **24**:633–642.
23. **Suzuki, K., A. Mori, K. J. Ishii, J. Saito, D. S. Singer, D. M. Klinman, P. R. Krause, and L. D. Kohn.** 1999. Activation of target-tissue immune-recognition molecules by double-stranded polynucleotides. Proc. Natl. Acad. Sci. U. S. A. **96**:2285–2290.
24. **Takaoka, A., Z. Wang, M. K. Choi, H. Yanai, H. Negishi, T. Ban, Y. Lu, M. Miyagishi, T. Kodama, K. Honda, Y. Ohba, and T. Taniguchi.** 2007. DAI (DLM-1/ZBP1) is a cytosolic DNA sensor and an activator of innate immune response. Nature **448**:501–505.
25. **Takeshita, F., K. J. Ishii, K. Kobiyama, Y. Kojima, C. Coban, S. Sasaki, N. Ishii, D. M. Klinman, K. Okuda, S. Akira, and K. Suzuki.** 2005. TRAF4 acts as a silencer in TLR-mediated signaling through the association with TRAF6 and TRIF. Eur. J. Immunol. **35**:2477–2485.
26. **Wang, Z., M. K. Choi, T. Ban, H. Yanai, H. Negishi, Y. Lu, T. Tamura, A. Takaoka, K. Nishikura, and T. Taniguchi.** 2008. Regulation of innate immune responses by DAI (DLM-1/ZBP1) and other DNA-sensing molecules. Proc. Natl. Acad. Sci. U. S. A. **105**:5477–5482.
27. **Yasutomo, K., T. Horiuchi, S. Kagami, H. Tsukamoto, C. Hashimura, M. Urushihara, and Y. Kuroda.** 2001. Mutation of DNASE1 in people with systemic lupus erythematosus. Nat. Genet. **28**:313–314.
28. **Yoshida, H., Y. Okabe, K. Kawane, H. Fukuyama, and S. Nagata.** 2005. Lethal anemia caused by interferon-beta produced in mouse embryos carrying undigested DNA. Nat. Immunol. **6**:49–56.

PCP
PLANT & CELL PHYSIOLOGY

Characterization of Receptor Proteins using Affinity Cross-linking with Biotinylated Ligands

Tomonori Shinya[1], Tomohiko Osada[1], Yoshitake Desaki[1], Masahiro Hatamoto[1], Yuko Yamanaka[2], Hisashi Hirano[2], Ryota Takai[3], Fang-Sik Che[3], Hanae Kaku[1] and Naoto Shibuya[1,*]

[1]Department of Life Sciences, School of Agriculture, Meiji University, Kawasaki, Kanagawa, Japan
[2]International Graduate School of Arts and Sciences, Yokohama City University, Yokohama, Kanagawa, Japan
[3]Graduate School of Bio-Science, Nagahama Institute of Bio-Science and Technology, Nagahama, Shiga, Japan
*Corresponding author: E-mail, shibuya@isc.meiji.ac.jp; Fax, +81-44-934-7039
(Received November 10, 2009; Accepted December 9, 2009)

Regular Paper

The plant genome encodes a wide range of receptor-like proteins but the function of most of these proteins is unknown. We propose the use of affinity cross-linking of biotinylated ligands for a ligand-based survey of the corresponding receptor molecules. Biotinylated ligands not only enable the analysis of receptor–ligand interactions without the use of radioactive compounds but also the isolation and identification of receptor molecules by a simple affinity trapping method. We successfully applied this method for the characterization, isolation and identification of the chitin elicitor binding protein (CEBiP). A biocytin hydrazide conjugate of *N*-acetylchitooctaose (GN8-Bio) was synthesized and used for the detection of CEBiP in the plasma or microsomal membrane preparations from rice and carrot cells. Binding characteristics of CEBiP analyzed by inhibition studies were in good agreement with the previous results obtained with the use of a radiolabeled ligand. The biotin-tagged CEBiP could be purified by avidin affinity chromatography and identified by LC-MALDI-MS/MS after tryptic digestion. We also used this method to detect OsFLS2, a rice receptor-like kinase for the perception of the peptide elicitor *flg*22, in membrane preparations from rice cells overexpressing OsFLS2. This work demonstrates the applicability of this method to the purification and identification of plant receptor proteins.

Keywords: Affinity labeling • Binding characteristics • Chitin oligosaccharide • Elicitor • One-step purification • Receptor.

Abbreviations: APEA, aminophenylethylamine; AzPEA, azidophenylethylamine; CEBiP, chitin elicitor binding protein; 2,5-DHBA, 2,5-dihydroxybenzonic acid; DTSSP, 3,3′-dithio*bis*[sulfosuccinimidyl propionate]; DTT, dithiothreitol; EGS, ethylene glycol *bis*[succinimidyl succinate]; GN7, *N*-acetylchitoheptaose; GN8, *N*-acetylchitooctaose; GN8-Bio, biotinylated *N*-acetylchitooctaose; HRP, horseradish peroxidase; MAMP, microbe-associated molecular pattern; PVDF, polyvinylidene difluoride; RLK, receptor-like kinase.

Introduction

Higher plants have the ability to recognize various chemical signals generated by other organisms as well as by themselves through perception by specific receptors that are present either on the cell surface or inside the cell. The identification of such receptors is essential to understanding the signaling cascade leading to a specific biological response, yet current knowledge on plant receptors is still limited. For example, the Arabidopsis and rice genomes are estimated to contain over 600 and 1200 receptor-like kinase (RLK) genes, respectively (Shiu et al. 2004), but only a handful of them are known for their functions and corresponding ligands.

Recently, several RLKs involved in the perception of microbe-associated molecular pattern (MAMP) elicitors, such as FLS2, EFR and CERK1, were identified and analyzed for their biological function (Gomez-Gomez and Boller 2000, Zipfel et al. 2006, Miya et al. 2007). Other RLKs, SR160 and PEPR1, were also identified as the receptors for the endogenous peptide elicitors systemin and *At*Pep1, respectively (Scheer and Ryan 2002, Yamaguchi et al. 2006). Similarly, BRI1 and PSKR1 were identified as the receptors for brassinosteroid and peptide hormones (Matsubayashi et al. 2002, Kinoshita et al. 2005). Receptors without kinase domains have also been reported, such as CEBiP for chitin elicitor (Kaku et al. 2006). Different strategies have been used to identify such receptor molecules. FLS2 and EFR, for example, were identified by screening mutants for the loss of response to the corresponding elicitor (Gomez-Gomez and Boller 2000, Zipfel et al. 2006). On the other hand, PSKR1 and CEBiP were purified by ligand-based affinity chromatography (Matsubayashi et al. 2002, Kaku et al. 2006). SR160 and PEPR1 were isolated by affinity-labeling of proteins (Scheer and Ryan 2002, Yamaguchi et al. 2006).

Regardless of the approaches used for the identification of the receptors, it is necessary to analyze their interaction with the corresponding ligands. One of the technical problems often associated with such analyses has been the use of radiolabeled

Plant Cell Physiol. 51(2): 262–270 (2010) doi:10.1093/pcp/pcp185, available online at www.pcp.oxfordjournals.org